Geochemistry, Geophysics, Geosystems

RESEARCH ARTICLE
10.1029/2019GC008308

Special Section:
Tethyan dynamics: from rifting to collision

Paleomagnetic Evidence for 25–15 Ma Crust Fragmentation of North Indochina (23–26°N): Consequence of Collision With Greater India NE Corner?

Fabio Speranza[1], Alessandra G. Pellegrino[2], Bo Zhang[3], Rosanna Maniscalco[2], Siyu Chen[3], and Catalina Hernandez-Moreno[1]

[1]Istituto Nazionale di Geofisica e Vulcanologia, Rome, Italy, [2]Dipartimento di Scienze Biologiche, Geologiche e Ambientali, Università degli Studi di Catania, Catania, Italy, [3]School of Earth and Space Science, Peking University, Beijing, China

Abstract The Cenozoic deformation of SE Asia is classically related to India-Asia collision and Tibet Plateau rise, supposedly resulting in the southeastward drift of lithospheric blocks bounded by strike-slip faults with displacements in the order of 1,000 km. Here we report on the paleomagnetism of 44 Triassic-Cretaceous red bed sites from the northern Simao, Chuandian, and Lanping "blocks," along both sides of the Ailao Shan-Red River shear zone (north Indochina). In the Simao domain, remagnetization predates folding and subsequent 48–70° clockwise rotation of three 2–5 km wide subblocks separated by two unrotated blocks. A primary magnetization component from the Lanping domain center suggests variably clockwise rotated (up to 95° ± 24°) sites, interrupted by a 2–6 km wide block that is rotated counterclockwise by 27° ± 6°. Thus, the Lanping and Simao "blocks" are far from being rigid, being made of a mosaic of independently deforming subblocks, whose kinematics and association with documented tectonics are speculative. It is unclear whether both folding and widespread remagnetization were synchronous or diachronous across north Indochina, but (considering previously published results) strike-slip activity along major shear zones, remagnetization, rotations, and crustal shortening overlapped within the 32–15 Ma time window, thus were likely genetically related. As opposed to previous models, we suggest that in early to mid-Cenozoic times, north Indochina was under the influence of oblique Neo-Tethys subduction. Collision between the NE corner of Greater India and Indochina at ~30 Ma yielded ENE-WSW shortening and strike-slip reactivation of preexisting faults, in turn fragmenting the crust into small, independently rotating, blocks.

Key Points:
- Paleomagnetism of Triassic-Cretaceous red beds from the Simao, Chuandian, and Lanping "blocks"
- "Blocks" are in fact brocken in 2-6 km wide sub-blocks rotating independently both CW and CCW
- Crust fragmentation of north Indochina related to collision with Greater India NE corner at ~30 Ma

Supporting Information:
- Supporting Information S1
- Table S1
- Table S2

Correspondence to:
F. Speranza,
fabio.speranza@ingv.it

Citation:
Speranza, F., Pellegrino, A. G., Zhang, B., Maniscalco, R., Chen, S., & Hernandez-Moreno, C. (2019). Paleomagnetic evidence for 25–15 Ma crust fragmentation of north Indochina (23–26°N): Consequence of collision with Greater India NE corner?. *Geochemistry, Geophysics, Geosystems*, *20*. https://doi.org/10.1029/2019GC008308

Received 5 MAR 2019
Accepted 22 AUG 2019
Accepted article online 06 NOV 2019

1. Introduction

In the 1970s, Peter Molnar and Paul Tapponnier proposed that the Cenozoic collision between India and Asia yielded the Tibet Plateau—the highest and widest High Plateau of Earth—and contemporaneous eastward extrusion of thickened crust, actively deforming all of E Asia (Molnar et al., 1973; Molnar & Tapponnier, 1975; Tapponnier & Molnar, 1977). Later, it was suggested that during Oligocene and Miocene times such deformation occurred through the E-SE directed lateral extrusion of several hundreds of km size megablocks—or proper "microplates"—bounded by transform faults with individual displacements of about 500–1,000 km (Leloup et al., 1995; Tapponnier et al., 1982, 1990).

On the other hand, the kinematics of present-day SE Asia deformation is clearly imaged by seismologic, geodetic, and geophysical data that image crust structure (Nelson et al., 1996; Socquet & Pubellier, 2005; Gan et al., 2007; Yao et al., 2008; Liang et al., 2013; Huang et al., 2017; Zhu et al., 2017; Figure 1). These data show that—at a large scale—the crust of E-SE Tibet may be viewed as a viscous fluid, floating east-southeastward above a very ductile lower-middle crust (Houseman & England, 1986, 1993). Lower-middle crust is assumed to flow above an undeformed mantle lid, while the megablock model for Cenozoic deformation required the occurrence of undeformed megablock interiors and coupled crust-upper mantle translation of the entire Asian lithosphere (e.g., Royden et al., 2008).

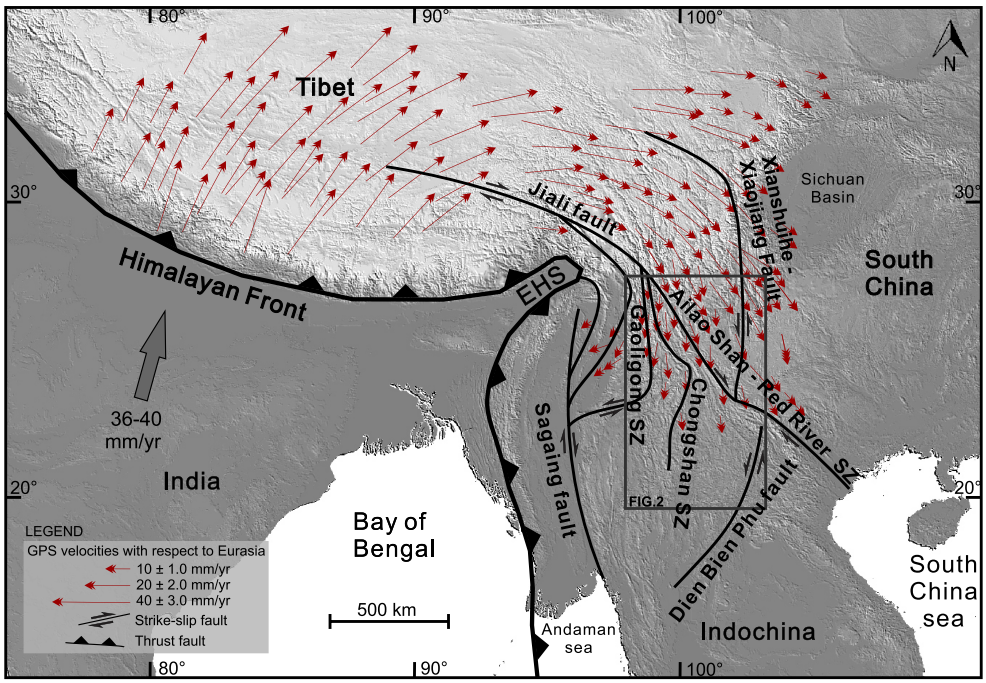

Figure 1. Schematic map of SE Asia showing active tectonics, generated by GIS (DEM source: Esri, User Community, geographic information system, Coordinate System & Projection: world geodetic system 1984-Web Mercator Auxiliary Sphere). The gray rectangle represents the study area (see Figure 2). Red thin arrows show present-day global positioning system velocities relative to stable Eurasia (e.g., Liang et al., 2013). EHS, East Himalayan Syntaxis; SZ, shear zone.

It is unclear whether the present-day SE Asia "thin viscous sheet" style of tectonism can be extrapolated to the geologic past, or if other models—such as the mega lithospheric block drift—apply. The history of India-Asia collision and Tibet thickening may extend back to 60–70 Ma (Zhu et al., 2017), and a clear change of tectonic regime in Indochina after mid Miocene (ca. 15 Ma) times has been widely reported (Burchfiel & Wang, 2003; Royden et al., 2008; Socquet & Pubellier, 2005; Wang, Zhang, et al., 2016). The pre-15 Ma Indochina deformation models should rely on geologic evidence—for example, offset estimate along the main strike-slip faults—that unfortunately have not yielded definitive conclusions so far. For example, displacement estimates reported for the well-studied Ailao Shan-Red River strike-slip shear zone (ARRSZ; Figure 1) vary greatly, from >1,000 km (Leloup et al., 1995) to unconstrained (Searle, 2006).

Paleomagnetism might represent a significant tool to address the question of pre-15 Ma SE Asia deformation style, as the size and kinematics of rotating blocks should better delineate crust fragmentation pattern. North Indochina is characterized by many continental basins where thick (up to 7 km) sequences of red beds—deposited during a long Triassic to Oligocene time window—were paleomagnetically investigated in the last 25 years (Figure 2 and Table S1 in the supporting information). Significant—mostly clockwise (CW) in sense—rotations with respect to stable Asia have been documented, but no consensus was reached so far on rotation pattern and rotating block size (e.g., Li, Advokaat, et al., 2017; Pellegrino et al., 2018).

In this paper we report paleomagnetic data from Upper Triassic-Lower Cretaceous red beds from the northern Simao, Chuandian and Lanping "blocks" from north Indochina (Figure 2). Forty-four new paleomagnetic sites, distributed along three transects orthogonal to the main strike-slip shear zones (ARRSZ and Chongshan shear zone) representing "block" boundaries, show that the Simao and Lanping "blocks" are in fact broken in small subblocks in the 2–5 km size order rotating independently during the 25–15 Ma time window. These new results call into question the mega-block (or "microplate") rotation/drift process inferred to occur in SE Asia during Cenozoic times.

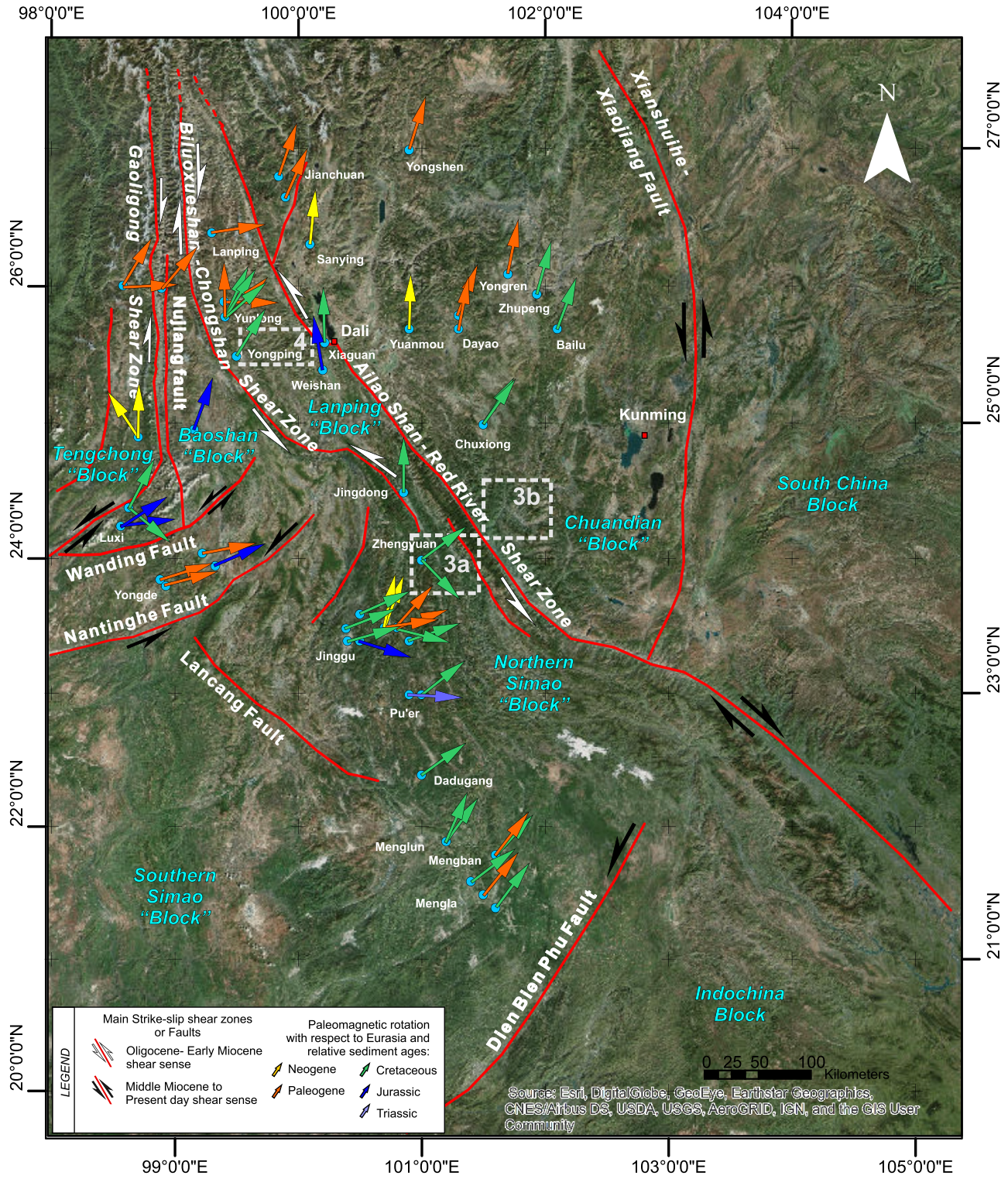

Figure 2. Map of north Indochina and surrounding regions, main tectonic features, and synthesis of previous paleomagnetic data. Base map source: GIS (Esri), World Geodetic System 1984-Web Mercator Auxiliary Sphere. Colored arrows (see legend) represent paleomagnetic rotations with respect to Eurasia, recalculated from previous paleomagnetic directions (see Table S1 in the supporting information), according to Demarest (1983) and using Eurasia (from 170 to 140 Ma) and East Asia (from 130 to 10 Ma) poles by Torsvik et al. (2012) and Cogné et al. (2013), respectively. The white boxes indicate the areas of paleomagnetic investigation (see Figures 3 and 4).

2. Geologic Setting

Crustal amalgamation of SE China occurred in middle-late Triassic times, when the South China Block collided with the Qinling orogen (Meng & Zhang, 1999). Afterward, apart for Jurassic times when marine sedimentation also occurred, Indochina was subjected to continental sedimentation that resulted into deposition of thick lower Jurassic-upper Oligocene red bed sequences. Deformation resumed during early-mid-Cenozoic times and was mainly characterized by ductile displacement along a few major N-S to NW trending shear zones—now exposing at their cores exhumed lower-middle crust rocks—that were supposed to separate less deformed and elongated "blocks" (hereinafter called "domains," Bureau of Geology and Mineral Resources of Yunnan Province, 1990; Bureau of Geology and Mineral Resources of Xizang Autonomous Region, 1993; Tapponnier et al., 1990; Leloup et al., 1995; Wang & Burchfiel, 1997; Akciz et al., 2008; Figure 2). From west to east, the Gaoligong, Biluoxueshan-Chongshan (hereinafter Chongshan), and ARRSZ separate the Tengchong, Baoshan, Lanping, and Chuandian domains. The Xianshuihe-Xiaojiang fault further separates the Chuandian domain from South China Block, but unlike other major structures shows a younger (post-10 Ma and ongoing) activity and does not expose lower crustal rocks in its core (Burchfiel & Wang, 2003; Wang et al., 1998). The Lanping domain grades at about 24.5°N latitude—without clear discontinuity—to the northern Simao domain, in turn separated from the Indochina domain by the Dien Bien Phu fault (Figure 2).

Several geochronologic/thermochronologic and structural geology investigations of the Gaoligong, Chongshan, and ARRSZ showed a long history of ductile compressive deformation starting as early as 60–55 Ma, followed by a main phase of strike-slip activity at 32–15 Ma, and final exhumation since 15 Ma (Leloup et al., 1995; Searle, 2006; Tapponnier et al., 1990; Zhang et al., 2010; Zhang, Zhang, Chang, et al., 2012; Zhang, Zhang, Zhong, et al., 2012; Zhang et al., 2017). After about 15 to 10 Ma, the shear zones became inactive or were reactivated/cut by brittle faults with kinematics that was opposite in sense to the previous Oligo-Miocene shear sense. The Gaoligong shear zone was characterized by dextral kinematics in the 32–10 Ma time windows, while no younger activity is documented in its central-northern N-S branch. The southern NE trending Gaoligong segment was reactivated as sinistral fault and yielded, in 1976, the M 7.4 Longling earthquake (Ekström et al., 2012). Similar recent and ongoing sinistral kinematics were documented in the subparallel and NE trending Wanding and Nantinghe faults (Figure 2). The Chongshan shear zone shows ductile deformation spanning a long, 57 to 16 Ma time window, with opposite dextral and sinistral strike-slip displacement reported for the 32–14 Ma time window along its northern and southern segment, respectively (Zhang et al., 2010; Zhang, Zhang, Chang, et al., 2012).

The ARRSZ is a major shear zone that received considerable attention since the 1980s, and was viewed by some authors as separating deforming and drifting Indochina from the stable South China Block. Ductile top-to-the-east midcrustal shortening took place during the 55–30 Ma window, followed by sinistral strike-slip shearing at 27–15 Ma, and younger E-W exhumation (Leloup et al., 1993, 1995, 2001; Tapponnier et al., 1990; Zhang et al., 2017). After about 10 Ma, the ARRSZ was reactivated as a brittle dextral fault yielding a cumulative $\leq$40 km displacement (Burchfiel & Wang, 2003; Schoenbohm et al., 2006; Wang et al., 1998; Wang, Zhang, et al., 2016).

The significance of the Oligo-Miocene left-lateral offset of the ARRSZ has been strongly debated. Tapponnier et al. (1990), Zhong et al. (1990), Leloup et al. (1995, 2007) and Li, Advokaat, et al. (2017)—mainly relying on displaced geological markers—considered it to represent the lithospheric boundary between the South China and Indochina blocks, and to be characterized by a left-lateral displacement of several hundreds of kilometers, possibly even exceeding 1,000 km. Relying on a review of available paleomagnetic data, Li, Advokaat, et al. (2017) also suggested that the displacement on the ARRSZ is ~600 km in the northwest, but only 250 km in the southeast. The 600–1,000 km displacement estimates would imply that the ARRSZ was a proper transform fault and that Indochina behaved as a microplate during Oligo-Miocene times. On the other hand, Searle (2006, 2007) recognized the ARRSZ as an Oligo-Miocene crustal strike-slip fault reactivating an older exhumed metamorphic core complex and stressed that the left-lateral offset cannot be estimated.

In comparison to previous shear zones, the Xianshuihe-Xiaojiang fault developed only in the last 10 Ma, with a brittle sinistral offset of ca. 60 km (Meade, 2007; Wang et al., 1998; Wang, Zhang, et al., 2016;

Zhang et al., 2004). It is interpreted as the present-day eastern boundary of SE extruding Tibetan crust, diverted to the south due to collision with rigid crust of the Sichuan Basin and South China Block (Figure 1).

Structural data from north Indochina relative to the ductile 55–20 Ma and fragile present-day deformation show a clear tectonic regime change, from a roughly E-W shortening direction (in present-day coordinates) during early-middle Cenozoic times to the N-S shortening direction evidenced at present by both active fault kinematics and focal mechanisms of major—mostly strike-slip—earthquakes (Ekström et al., 2012; Pellegrino et al., 2018; Socquet & Pubellier, 2005; Zhang et al., 2017; Zhang, Zhang, Chang, et al., 2012). This observation, coupled with GPS data showing a southward drift of north Indochina at a ~2 cm/year rate (Gan et al., 2007; Liang et al., 2013) and with evidence for hot—and likely partially molten—lower crust below E-SE Tibet (Nelson et al., 1996; Yao et al., 2008), suggests that active north Indochina deformation is driven by lower crust flowing southeastward in-between the rigid crustal buttresses represented by the East Himalayan Syntaxis and the Sichuan basin (Figure 1; Royden et al., 1997, 2008).

The north Indochina and Chuandian domains mainly expose spectacular sequences of continental red beds —mostly Jurassic-Oligocene in age—locally exceeding a 7 km thickness (Bureau of Geology and Mineral Resources of Yunnan Province, 1990). Discontinuous exposures of Miocene-Pleistocene sediments and deposits are scattered throughout the area, and unconformably overlie the red bed sedimentary sequences.

At some localities red beds are intensely deformed, with fold axes that are roughly parallel to shear zones approaching them, and complex and apparently multiphase deformation patterns seem to occur at "block" centers (dome-like tectonic structures are observed within the Lanping domain). The age of folding is not well determined, and deformation probably occurred with variable magnitude over a long time span, starting as early as mid-Eocene (ca. 45 Ma) in the southern part of the Simao domain near the China-Laos border (e.g., Wang et al., 1998; Wang & Burchfiel, 1997). However, the age of deformed red bed sequences and the shallow attitude of mid Miocene and younger sedimentary deposits point to a main phase of late Oligocene to early Miocene (25–15 Ma) compressional deformation, at least for the Lanping-Simao domains north of 22°N (Bureau of Geology and Mineral Resources of Yunnan Province, 1990; He et al., 1996).

2.1. Previous Paleomagnetic Research in North Indochina

The recognition of active crustal deformation of East Asia (Molnar et al., 1973), the suggestion of lateral microplate extrusion due to India-Eurasia collision (Tapponnier et al., 1982, 1990), and the widespread occurrence of red beds well suitable for paleomagnetic investigation, stimulated, since the early 1990s, many paleomagnetic studies in north Indochina. In Figure 2, we show rotation estimates from north Indochina and the Chuandian domain with respect to stable Eurasia, reevaluated using reference Eurasia paleopoles by Torsvik et al. (2012) for sites in 170 to 140 Ma values, and the most recent East Asia-based poles summarized by Cogné et al. (2013) for sites in 130 to 10 Ma values. Data (and the complete list of papers) from the Lanping, north Simao, and Chuandian domains are given in Table S1 (see supporting information), while revised data from the Baoshan and Tengchong domains were recently reported by Pellegrino et al. (2018).

Figure 2 shows a general predominance of variable magnitude CW rotations from Jurassic-Oligocene rocks, and Neogene sediments and deposits show barely significant rotations. The Chuandian domain yields a rather clear pattern of 15–20° CW rotations for Cretaceous-Oligocene red beds (Funahara et al., 1992; Gao et al., 2017; Li et al., 2013, 2015; Otofuji et al., 1998; Tong et al., 2015; Wang, Yang, et al., 2016; Yang, Sun, et al., 2001; Yoshioka et al., 2003; Zhu et al., 2008). Jurassic-Oligocene red beds from the Baoshan, Lanping, and northern Simao domains provide highly variable CW rotations, in few cases exceeding 90° (Chen et al., 1995; Funahara et al., 1993; Gao et al., 2015; Huang & Opdyke, 1993, 2015; Kondo et al., 2012; Li, Yang, et al., 2017; Li et al., 2018; Sato et al., 1999, 2001, 2007; Tanaka et al., 2008; Tong et al., 2013, 2016; Yang, Yin, et al., 2001; Yang, Sun, et al., 2001). In the Tengchong domain, both CW and counterclockwise (CCW) rotations have been documented (Kornfeld et al., 2014a, 2014b).

The inhomogeneous pattern of tectonic rotations of north Indochina is likely also related to remanence acquisition complexities in red beds. In fact, several paleomagnetic studies have shown that detrital hematite (or specularite) in red beds, which may carry a primary magnetization, competes with hematite precipitation and growth during subsequent hydrothermal fluid circulation, frequently yielding a very stable chemical remanent magnetization (CRM) and secondary magnetization overprint (Collinson, 1966; Walker et al., 1981; Kent et al., 1986; Liu et al., 2011; Jiang et al., 2015, 2017, among many others). Several paleomagnetic

studies of north Indochina red beds report a paleomagnetic overprint—inferred by the occurrence of ubiquitous normal polarities in rocks of wide age ranges—coupled with a positive fold test, suggesting a pretilting (i.e., pre-25–15 Ma) remagnetization (Funahara et al., 1993; Gao et al., 2015, 2017; Li, Yang, et al., 2017; Sato et al., 1999, 2007). However, other studies reported also dual polarities, and isolated a (presumably primary) remanence unblocked at very high temperatures, in the 610–670 °C to 690 °C temperature range (Chen et al., 1995; Huang & Opdyke, 1993; Kondo et al., 2012; Sato et al., 2001; Tanaka et al., 2008; Tong et al., 2013, 2015, 2016; Wang, Yang, et al., 2016; Yoshioka et al., 2003).

Most of the published paleomagnetic studies (Funahara et al., 1993; Huang & Opdyke, 1993, 2015; Li, Advokaat, et al., 2017; Li et al., 2018; Otofuji et al., 2010; Tong et al., 2016) associate the CW rotations to the eastward drifting microplate model put forward by Tapponnier et al. (1982, 1990), identifying each shear zone-bounded domain with a rigid rotating block. However, a major problem of space would arise if one assumes that the N-S elongated Baoshan and Lanping domains rotated CW by some 80°, questioning the internal block rigidity and appropriate delineation of a tectonic block. Other studies (Kornfeld et al., 2014a, 2014b; Li et al., 2018; Otofuji et al., 2010; Sato et al., 1999; Tong et al., 2017) relate the CW rotations to rotational southeastward displacement of crust around the East Himalaya Syntaxis, similar to the present geodetic pattern (Figure 1; Liang et al., 2013). However, the documented paleomagnetic rotations are mostly pre-middle-Miocene (i.e., pre-15 Ma) in age, so that present-day CW rotations shown by GPS data can hardly be related to the pattern of paleomagnetic rotations.

Although the microplate/megablock model prevailed in the paleomagnetic literature on northern Indochina, some papers indeed recognized the possibility of "internal" block deformation and local rotations, due to oroclinal bending of fold axes (Gao et al., 2015; Kondo et al., 2012; Yoshioka et al., 2003), or small blocks decoupled by an array of strike-slip faults according to the "domino" model by McKenzie and Jackson (1986) (Otofuji et al., 2012; Tanaka et al., 2008; Tsuchiyama et al., 2016; Wang et al., 2008). It is worth noting that Funahara et al. (1993), Huang and Opdyke (1993), Sato et al. (2001), and Tanaka et al. (2008) documented in the Lanping domain a few sites carrying a pretilting magnetization (primary magnetization as inferred by dual magnetic polarities in two cases) that implied little if any rotation (Figure 2). Such data indeed question the definition of rigid and internally coherent CW rotating "blocks" in north Indochina.

Recently, Pellegrino et al. (2018) documented a pattern of decreasing CW rotation values (from 165° to nearly 0) within a distance of 20 km east of the Gaoligong shear zone, revealing that fault shear can be a significant source of local rotations. This study showed that—in the vicinity of the Gaoligong shear zone—the crust is broken in 1 km size crust fragments, conforming to a quasi-continuous crust deformation model (Sonder et al., 1994). However—as also Pellegrino et al. (2018) admit—"blocks" between major shear zones are up to 200 km wide (in case of the north Simao domain), implying that fault shear cannot be the sole mechanism for the widespread CW rotations documented in northern Indochina.

3. Sampling and Methods

We collected 443 paleomagnetic samples from forty-four sites (routinely 10 samples per site) along three crust transects orthogonal to the ARRSZ and at both margins of it (Figures 2–4), trying to spread sites as much as possible along each transect. All sites were sampled in Upper Triassic to Lower Cretaceous continental red beds that were shown by previous studies to give valuable paleomagnetic information. Sixteen sites (Yun51-66) were distributed in the northern Simao domain, from the Silurian-Triassic sediment contact to a maximum 31 km distance from ARRSZ mylonites (Figure 3a). East of the ARRSZ, nine sites (Yun67-75) were sampled in the Chuandian domain, up to a maximum 36 km from shear zone mylonites (Figure 3b). In the Lanping block, 19 sites (Yun76-94) were distributed along a WSW-ENE transect from the Chongshan to the ARRSZ (Figure 4).

The samples from each site, which is intended to represent a geographically distinct locality, were distributed as much as possible on different beds from a given outcrop to attempt to average out paleosecular variation of the geomagnetic field. Therefore, each site represents in fact a paleomagnetic pole and can be directly compared to coeval reference poles from stable Eurasia.

Each sample was taken by drilling a core with a petrol-powered portable drill cooled by water and orienting it in situ using Sun (when possible) and a magnetic compass, corrected for the local magnetic declination for

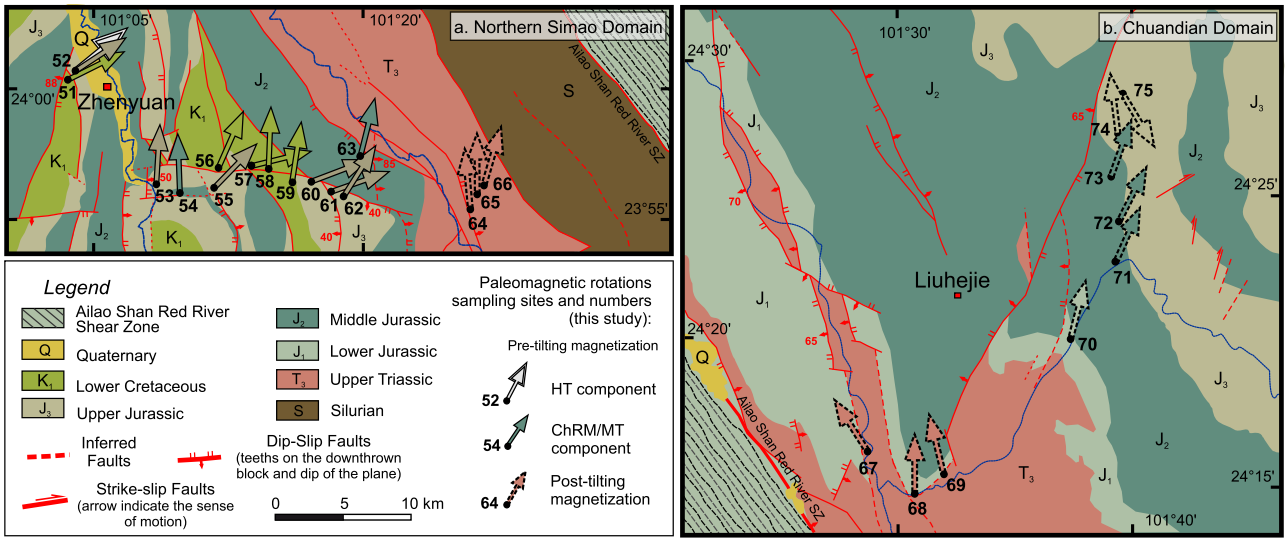

Figure 3. Paleomagnetic rotations with respect to Asia from the northern Simao (a) and Chuandian (b) domains (geological base map modified after Bureau of Geology and Mineral Resources of Yunnan Province, 1990). Solid contour arrows show the rotation values with respect to tilt-corrected characteristic/medium temperature (ChRM/MT) paleomagnetic directions and pretilting normal polarity remagnetization (30 Ma Asia paleopole; see text). The rotation of reverse polarity high temperature (HT) component from site Yun52 was also calculated with respect to 150 Ma paleomagnetic pole, coeval to sediment age. Dashed arrows are rotation values relative to in situ paleomagnetic directions (posttilting secondary magnetizations).

year 2017 (1°W according to the National Oceanic and Atmospheric Administration's National Geophysical Data Center, http://www.ngdc.noaa.gov/geomag/declination.shtml).

The sampled cores were cut into standard cylindrical paleomagnetic specimens of 22 mm height, and the paleomagnetic measurements were carried out in the shielded room of the paleomagnetic laboratory of the Istituto Nazionale di Geofisica e Vulcanologia (Roma), using a 2G Enterprises direct current superconducting quantum interference device cryogenic magnetometer.

All samples were thermally demagnetized using a Pyrox shielded oven in 12 temperature steps up to 680 °C. Demagnetization data were plotted on orthogonal vector component diagrams (Zijderveld, 1967). The magnetization components were identified by principal component analysis (Kirschvink, 1980), and the site-mean paleomagnetic directions were computed using Fisher (1953) statistics and plotted on equal-angle projections. Finally, the rotation and flattening values with respect to Eurasia were evaluated according to Demarest (1983), using the recent and East Asia-focused poles by Cogné et al. (2013) that extend to 130 Ma (Eurasia paleopoles by Torsvik et al., 2012, were used for sites with magnetizations presumably acquired in older times). To define the sense and amount of rotation, we always considered the smaller of the two angles between the observed and expected declinations, thus calculating rotation values $\leq|180°|$. This is a conservative approach, although we are aware that—mostly in the vicinity of strike-slip faults—rotations may possibly exceed 180° (e.g., Hernandez-Moreno et al., 2014; Nelson & Jones, 1987; Piper et al., 1997).

Moreover, one specimen per site was selected to carry out additional analyses with the aim of characterizing the magnetic mineralogy. Following Lowrie (1990), we thermally demagnetized up to 680 °C a composite isothermal remanent magnetization (IRM) acquired by applying subsequently a 2.7, 0.6, and 0.12 T magnetic field along the *z*, *y*, and *x* sample axes (respectively).

3.1. Paleomagnetic Results and Fold Tests

Apart from a viscous component typically unblocked by 300 °C (Figure 5), three main thermal demagnetization behaviors are observed. In ~5% of the samples, a characteristic magnetization component (ChRM) is observed in the 300–600 °C temperature interval, followed by erratic magnetization changes and an increase in intensity, suggesting the growth of newly formed magnetic minerals (Figures 5a and 5k). In most of the samples (~65%, mostly from the north Simao and Chuandian domains), a ChRM is isolated in the 300–680 °C temperature range (Figures 5c, 5d, 5f, 5g, and 5l). In ~30% of the samples (mostly from the

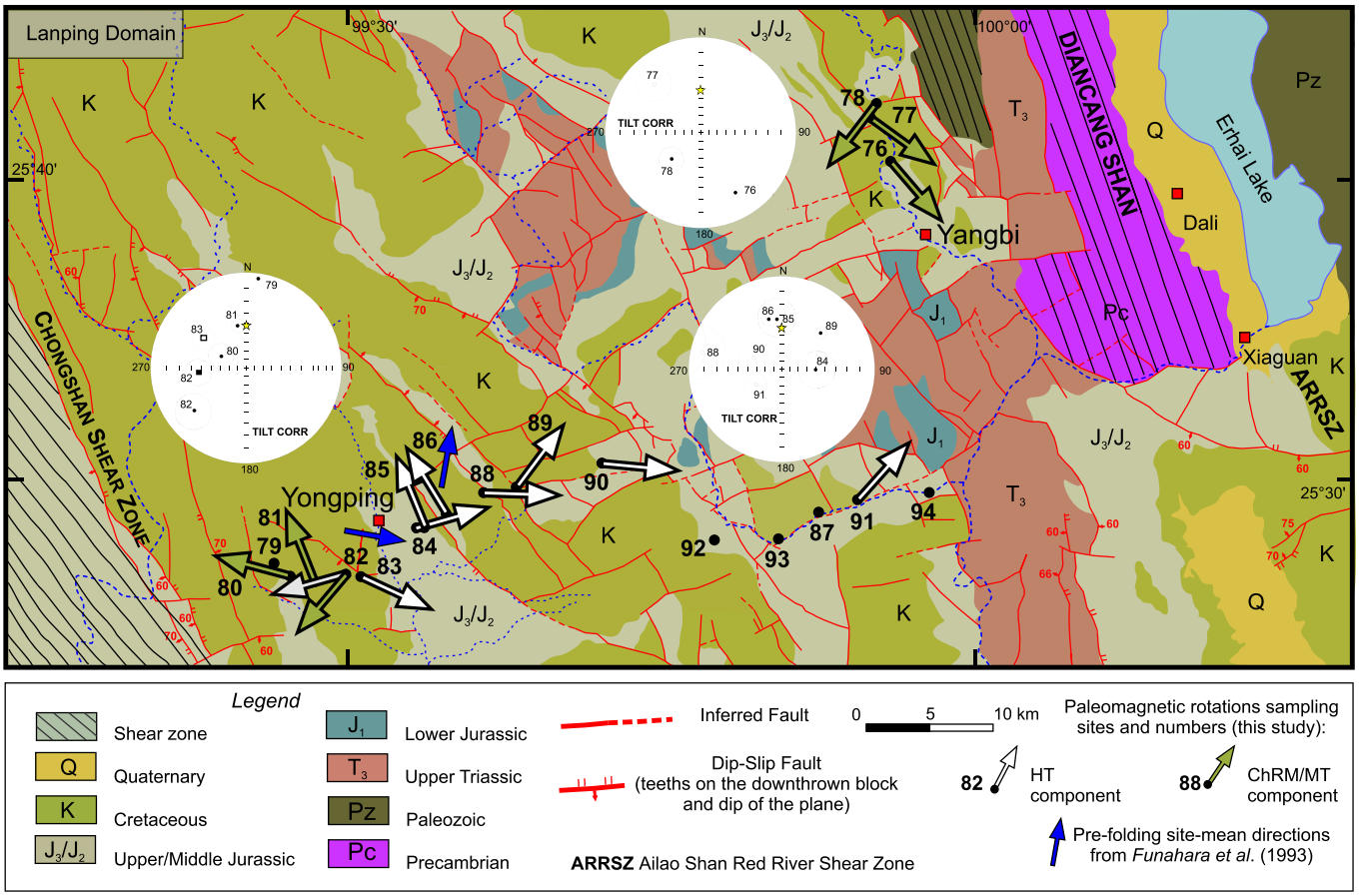

Figure 4. Estimated paleomagnetic rotations with respect to Asia from the Lanping domain (geologic map modified after Bureau of Geology and Mineral Resources of Yunnan Province, 1990). White and green arrows show the rotations evaluated based on high temperature (HT) and characteristic (ChRM) magnetization components, respectively. The medium temperature (MT) components, shown to have undergone an overprint at 28% unfolding and no further rotation (see text), are omitted. Equal-angle projections of the tilt-corrected paleomagnetic directions from the corresponding sites are also shown. Averages of three and five prefolding site-mean directions reported by Funahara et al. (1993) just west and east of Yongping (respectively) are also shown.

Lanping domain) a medium (MT) and high temperature (HT) component are isolated in the 300–640 and 640–680 °C temperature ranges, respectively (Figures 5b, 5e, 5h, 5i, 5j, and 5n).

We make clear that the HT components were calculated by connecting only two demagnetization points (640 and 680 °C); thus, we admit that the HT component directions of our data set may be slight biased. However, several studies of red beds from Indochina have showed that the HT component is usually defined at a temperature range varying between 600–680 °C and 640–680 °C, never found to be higher than 670–690 °C (Chen et al., 1995; Huang & Opdyke, 1993; Kondo et al., 2012; Sato et al., 2001; Tanaka et al., 2008; Tong et al., 2013, 2015, 2016; Wang, Yang, et al., 2016; Yoshioka et al., 2003). Figure 5 shows that—considering samples where a HT occurs—remanence directions change slightly from 600 to 640 °C, testifying the final unblocking of the MT components. We conclude that a HT defined from an undetermined temperature range between 640–680 °C and 670–680 °C would not be significantly different from the HT component determined by us in the 640–680 °C temperature range.

The composite IRM results show that most of the IRM is unblocked along the high and intermediate-coercivity (2.7–0.12 T) axes and is fully unblocked at 680 °C (Figure S1 in the supporting information). Thus, all paleomagnetic data show the almost exclusive occurrence of hematite with variable grain size as remanence carrier, consistently with previous evidence from red beds sampled in the same region (Funahara et al., 1993; Huang & Opdyke, 1993, 2015; Li, Yang, et al., 2017; Otofuji et al., 2010, 2012; Sato et al., 2001; Tanaka et al., 2008; Tong et al., 2016; Wang et al., 2008).

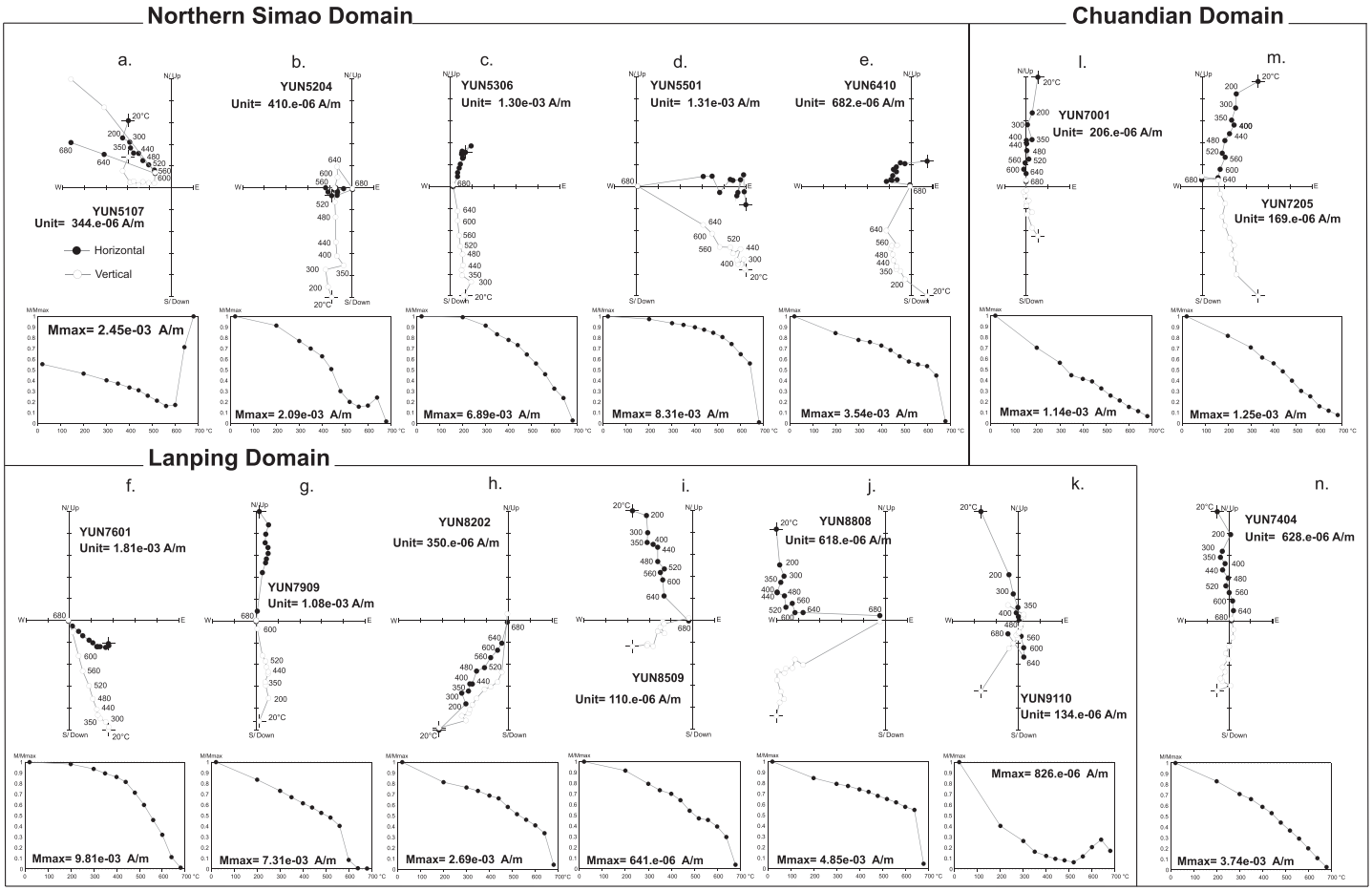

Figure 5. Orthogonal vector diagrams of typical thermal demagnetization data (in situ coordinates) showing response to demagnetization by representative samples carrying characteristic (ChRM), medium temperature (MT) or high temperature (HT) components. Solid (open) symbols represent projections onto the horizontal (vertical) plane. Demagnetization step values are in degrees Celsius.

Estimated mean paleomagnetic directions from all sites are reported in Table 1. Jurassic-Cretaceous directions from the north Simao domain were obtained by averaging ChRMs and MT components, with the exception of site Yun52, where both MT and HT mean directions could be identified (Figure 6). The paleomagnetic directions from samples collected in the Triassic strata were evaluated by averaging MT components, because HT directions were scattered (Table 1). In the Chuandian domain, MT and ChRMs were averaged out, as the few and small intensity HT components were scattered and/or not sufficient in calculating a site-mean direction. In the Lanping domain, two different behaviors characterize the sites located at domain edges (within a 13 km distance from the ARRSZ and Chongshan shear zones), and sites from domain center (Figure 7). Sites at domain edges yield site-mean directions calculated by averaging ChRMs (Figures 5f and 5g), while only at site Yun82-83 both MT and HT directions were isolated (Figure 5h). Sites from Lanping domain center yielded mean MT and HT directions at eight and seven sites, respectively (Figure 7 and Table 1).

Site-mean directions are usually well determined, with α_{95} values varying from 1.8° to 20.5° (11.0° on average). All sites from the Simao and Chuandian domains (except the HT component of site Yun52) and all MT components from the Lanping domain yield a normal polarity, while both normal and reverse polarity magnetizations are resolved in the remaining sites. The reversal test could not be applied on the entire population of results, as directions are clearly not antipodal due to significant rotations of the individual sites (Figures 6 and 7).

The fold test according to McFadden (1990) was applied separately on sites from each domain, and the results are provided in Table S2 (see supporting information). Directions from the Simao domain

Geochemistry, Geophysics, Geosystems

10.1029/2019GC008308

Table 1
Paleomagnetic Directions From Red Beds From the Northern Simao, Chuandian, and Lanping Domains (Northern Indochina)

Site	Geographic coordinates		Age	Age (Ma)	Considered palepoles age (Ma)	Demagnetization component	Bedding (deg)	n/N	In situ		Tilt corrected		k	α95 (deg)	R (deg)	ΔR (deg)	F (deg)	ΔF (deg)
	Latitude ° N	Longitude ° E							D (deg)	I (deg)	D (deg)	I (deg)						
Northern Simao Domain																		
YUN51	24°00′36.8″	101°04′47.8″	LK	100–145	30	ChRM	105/109	7/10	306.2	10.7	68.2	53.7	34.2	10.5	65.9	14.2	−20.2	8.9
YUN52	24°00′39.6″	101°05′12.6″	UJ	145–163	30	MT	61/51	9/10	240.5	71.5	61.3	57.5	58.7	6.8	58.9	10.2	−24.0	6.3
					150	HT		9/10	256.8	−68.1	247.1	−17.8	17.0	12.8	50.7	12.1	35.0	11.3
YUN53	23°56′26.8″	101°08′43.3″	UJ	145–163	30	ChRM	7/41	10/10	9.9	70.3	8.2	29.3	713.2	1.8	5.8	2.8	4.1	3.6
YUN54	23°55′57.0″	101°09′59.6″	MJ	163–174	30	ChRM	50/30	8/10	342.2	46.4	2.6	29.8	40.9	8.8	0.2	8.2	3.6	7.6
YUN55	23°56′22.3″	101°11′17.3″	UJ	145–163	30	ChRM	260/54	9/10	60.2	−0.5	48.8	49.1	46.3	7.6	46.4	9.4	−15.7	6.8
YUN56	23°56′56.3″	101°11′31.9″	LK	100–145	30	ChRM	33/56	10/10	283.7	86.1	28.5	35.2	49.4	6.9	26.1	7.0	−1.8	6.4
YUN57	23°57′06.9″	101°12′41.4″	LK	100–145	30	ChRM	76/81	9/10	252.0	45.0	80.8	53.8	224.6	3.4	78.4	5.0	−20.4	4.3
YUN58	23°56′55.6″	101°13′31.7″	LK	100–145	30	ChRM	10/70	9/10	201.8	77.1	6.9	32.6	52.1	7.2	4.5	7.1	0.8	6.6
YUN59	23°56′23.2″	101°14′34.6	LK	100–145	30	ChRM	348/31	9/10	38.8	64.7	13.4	39.5	66.7	6.4	11.0	6.9	−6.1	6.0
YUN60	23°56′25.8″	101°14′57.7″	UJ	145–163	30	MT	257/54	10/10	74.5	−15.0	73.9	39.0	24.9	9.9	71.5	10.2	−5.6	8.4
YUN61	23°56′00.4″	101°16′22.8″	UJ	145–163	30	ChRM	5/46	10/10	108.3	35.1	75.5	32.4	102.8	4.8	73.1	5.0	1.0	5.0
YUN62	23°55′53.2″	101°16′38.7″	UJ	145–163	30	ChRM	24/11	9/10	41.9	64.3	37.0	53.7	118.3	4.8	34.6	6.7	−20.3	5.0
YUN63	23°57′11.5.0″	101°17′35.5″	MJ	163–174	30	ChRM	266/56	9/10	41.5	7.2	18.8	41.1	75.3	6.0	16.4	6.6	−8.2	5.8
YUN64[a]	23°55′27.5″	101°22′21.3″	UT	201–237	30	MT	184/55	9/10	357.0	71.2	187.8	53.6	17.3	12.7	−5.4	33.6	−37.8	10.5
YUN65[a]	23°56′09.7″	101°22′33.8″	UT	201–237	30	MT	5/80	10/10	2.1	49.8	2.9	−30.1	27.7	9.3	−0.3	11.5	−16.4	8.0
YUN66[a]	23°56′15.9″	101°22′44.1″	UT	201–237	30	MT	294/114	6/10	18.7	51.3	336.0	−21.7	30.6	12.3	16.3	15.7	−17.9	10.2
Chuandian domain																		
YUN67[a]	24°15′08.5″	101°28′44.3″	UT	201–237	20	ChRM	_	10/11	329.6	25.4	_	_	19.8	11.1	−32.8	9.9	9.8	9.4
YUN68[a]	24°13′33.6″	101°30′47.7″	UT	201–237	20	ChRM	290/26	6/10	2.3	39.3	346.4	27.7	11.7	20.4	−0.1	21.0	−4.1	16.3
YUN69[a]	24°14′26.2″	101°31′53.9″	UT	201–237	20	ChRM	118/29	6/10	348.7	53.0	34.6	62.1	11.6	20.5	−13.7	27.9	−17.8	16.4
YUN70[a]	24°19′10.4″	101°37′20.9″	LJ	174–201	20	ChRM	66/31	8/10	16.8	36.3	27.1	13.6	29.8	10.3	14.4	10.3	−1.0	8.8
YUN71[a]	24°21′59.7″	101°38′47.1″	MJ	163–174	20	ChRM	69/45	7/10	26.3	80.8	61.1	38.0	18.6	14.4	23.9	14.2	−45.4	14.4

Geochemistry, Geophysics, Geosystems

10.1029/2019GC008308

Table 1
(continued)

Site	Geographic coordinates		Age	Age (Ma)	Considered palepoles age (Ma)	Demagnetization component	Bedding (deg)	*n*/*N*	In situ		Tilt corrected		*k*	α95 (deg)	*R* (deg)	Δ*R* (deg)	*F* (deg)	Δ*F* (deg)
	Latitude ° N	Longitude ° E							*D* (deg)	*I* (deg)	*D* (deg)	*I* (deg)						
YUN72[a]	24°24′08.8″	101°39′ 42.9″	MJ	163–174	20	MT	80/47	9/10	29.0	55.7	52.7	17.7	33.1	9.1	26.6	13.0	−20.2	8.0
YUN73[a]	24°26′12.2″	101°39′ 24.7″	MJ	163–174	20	MT	61/50	7/10	21.9	71.7	48.3	25.1	11.8	18.3	19.5	70.2	−36.2	14.7
YUN74[a]	24°27′19.3″	101°39′ 34.2″	UJ	145–163	20	ChRM	68/36	7/10	355.1	39.7	15.2	22.6	28.7	11.4	−7.3	11.9	−4.2	9.6
YUN75[a]	24°29′15.0″	101°39′ 49.1″	UJ	145–163	20	MT	12/74	7/10	154.2	59.1	35.7	38.8	67.0	7.4	151.8	11.6	−23.5	6.8
Lanping domain																		
YUN76	25°43′20.7″	099°55′ 31.2″	LK	100–145	120	ChRM	162/57	10/10	123.0	71.4	149.8	18.0	212.3	3.3	139.4	3.7	24.8	3.9
YUN77	25°45′05.9″	099°54′ 44.2″	LK	100–145	120	ChRM	342/29	9/10	317.7	6.3	316.2	−20.1	13.6	14.5	125.8	12.3	22.8	11.7
YUN78	25°45′43.0″	099°54′ 41.6″	LK	100–145	120	ChRM	193/60	8/10	322.6	58.9	227.7	45.5	19.8	12.8	−142.6	14.6	−3.1	10.4
YUN79[a]	25°26′14.1″	099°26′ 31.1″	LK	100–145	20	ChRM	21/38	8/10	3.7	40.1	7.8	3.3	811.9	1.9	5.5	3.0	33.6	3.8
YUN80	25°25′44.7″	099°27′ 06.5″	LK	100–145	120	ChRM	101/24	7/10	290.1	34.6	295.3	58.1	19.4	14.0	−75.0	21.4	−15.7	11.3
YUN81	25°25′28.5″	099°28′ 24.0″	LK	100–145	120	ChRM	331/48	8/10	64.5	76.8	348.6	41.4	69.6	6.7	−21.7	7.4	0.9	6.0
YUN82	25°25′35.9″	099°30′ 01.3″	LK	100–145	120	MT	297/51	8/10	205.1	30.4	230.5	19.9	15.8	14.4	−139.8	12.2	22.4	11.6
					120	HT		8/10	200.8	64.6	264.6	37.2	17.0	12.7	−105.7	12.7	5.2	10.3
YUN83	25°25′23.1″	099°30′ 57.6″	LK	100–145	120	HT	50/40	9/10	333.0	−33.5	305.4	−32.9	25.3	10.4	115.1	10.0	9.4	8.6
YUN84[b]	25°27′56.0″	099°33′ 17.6″	UJ	145–163	20	MT	117/94	9/10	319.3	12.7	(325.1)	(38.1)	14.9	13.8	−37.2	14.0	−1.2	11.3
					150	HT		8/10	316.5	31.5	90.8	49.9	8.7	19.9	73.9	25.6	3.9	16.3
YUN85[b]	25°27′49.3″	099°33′ 41.6″	UJ	145–163	20	MT	75/55	9/10	355.9	51.3	(13.2)	(45.9)	10.1	17.0	10.9	19.5	−9.0	13.7
					150	HT		8/10	320.8	25.4	354.6	33.3	10.1	18.1	−22.3	18.7	20.5	15.5
YUN86	25°28′16.2″	099°34′ 42.2″	UJ	145–163	150	HT	86/53	9/10	324.3	11.2	345.5	31.9	55.1	7.0	−31.4	8.8	21.9	7.5
YUN87[b]	25°28′11.2″	099°52′ 09.6″	LK	100–145	20	MT	115/65	9/10	343.9	27.7	(354.1)	(39.0)	18.4	12.3	−8.2	12.7	−2.1	10.2
YUN88[b]	25°29′21.7″	099°36′ 26.9″	LK	100–145	20	MT	252/28	8/10	0.6	29.4	(356.0)	(31.6)	10.4	18.0	−6.3	16.8	5.3	14.5
					120	HT		7/10	283.1	16.2	282.1	−8.0	12.0	18.1	91.8	14.5	34.5	14.4
YUN89	25°29′24.4″	099°38′ 09.6″	LK	100–145	120	HT	22/71	10/10	143.6	64.6	47.1	30.5	80.3	5.4	36.8	5.5	11.9	5.2
YUN90	25°30′52.2″	099°41′ 15.1″	UJ	145–163	150	HT	275/50	8/10	284.8	−6.5	292.3	−55.4	12.0	16.5	95.4	24.2	−1.5	13.8

Table 1
(continued)

Site	Geographic coordinates		Age	Age (Ma)	Considered (Ma)	paleopoles age	Demagnetization component	Bedding (deg)	n/N	In situ		Tilt corrected		k	α95 (deg)	R (deg)	ΔR (deg)	F (deg)	ΔF (deg)
	Latitude ° N	Longitude ° E								D (deg)	I (deg)	D (deg)	I (deg)						
YUN91[b]	25°28′36.2″	099°54′08.4″	LK	100–145	20		MT	135/85	9/11	8.1	19.9	(18.9)	(33.2)	8.0	19.4	16.6	18.4	3.7	15.5
					120		HT		9/11	170.3	−12.0	238.7	−54.4	17.7	12.6	41.9	18.2	−0.5	11.1
YUN92[b]	25°27′12.7″	099°47′08.9″	UJ	145–163	20		MT	262/53	9/10	9.2	44.5	(352.8)	(47.1)	40.4	8.2	−9.5	9.8	−10.2	7.3
YUN93[b]	25°27′09.4″	099°50′24.9″	LK	100–163	20		MT	120/57	8/10	341.9	16.4	(346.9)	(28.6)	35.8	9.4	−15.4	8.8	8.3	8.1
YUN94[b]	25°29′03.7″	099°57′02.7″	MJ	163–174	20		MT	276/45	8/10	354.6	41.1	(344.4)	(37.3)	37.0	9.2	−17.9	9.4	−0.3	8.0

Note. Ages: UT, Upper Triassic; LJ, Lower Jurassic; MJ, Middle Jurassic; UJ, Upper Jurassic; LK, Lower Cretaceous. Demagnetization component: ChRM, characteristic remanent magnetization (300–680 °C); MT, medium temperature (300–640 °C) component; HT, high temperature component (640–680 °C). The geographic coordinates are referred to WGS84 datum. Age in Ma is from the geologic timescale of Cohen et al. (2013). Bedding is expressed in dip azimuth/dip values. *D* and *I* are site mean declination and inclination calculated before and after tectonic correction; *k* and α95 are statistical parameters after Fisher (1953); *n*/*N* is number of samples giving reliable results/number of studied samples at a site. Site mean rotation *R* and flattening *F* values, and relative errors Δ*R* and Δ*F* (according to Demarest, 1983) are relative to coeval *D* and *I* Eurasian values expected at the sampling area considering Eurasian paleopoles from Cogné et al. (2013), or Torsvik et al. (2012) for poles older than 150 Ma.
[a]Posttilting remagnetized sites; *R* and *F* values are calculated using the in situ *D* and *I* values. [b]Syntilting remagnetized sites; the *R* and *F* values are calculated using the *D* and *I* values obtained at 30% unfolding (in parentheses).

(excluding results from the three Triassic sites) support a positive fold test at the 99% significance level, while data from the three Triassic sites and sites from the Chuandian domain yield a negative fold test. Conversely, a rather complex behavior is shown by data from sites in the Lanping domain (excluding the three scattered sites sampled close to the ARRSZ). Sites sampled close to the Chongshan shear zone (but site Yun79) yield indeterminate fold test results. Site Yun79 shows an in situ direction that is nearly coincident with the local geocentric axial dipole field direction, and a tilt-corrected subhorizontal direction of remanence (Figure 7); thus, it was considered as recently remagnetized and excluded from further consideration. Conversely, HT directions from the Lanping domain center support a positive fold test, while the MT directions appear to have been acquired at about 30% unfolding (Figure 7).

3.2. Magnetization Origin and Overprint Age

According to available geologic maps (Bureau of Geology and Mineral Resources of Yunnan Province, 1990), sites from the north Simao domain (excluding the three sites in Triassic rocks) involve rocks of Middle Jurassic-Early Cretaceous age, and the time period is characterized by several normal and reverse polarity chrons (Gradstein et al., 2012). However, all sites (except the HT component of site Yun52) yield a normal polarity remanence, strongly suggesting a prefolding magnetization overprint (that still results in a positive fold test). A similar normal polarity, pretilting secondary magnetization has been documented in other studies of Jurassic-Oligocene red beds from north Indochina (Funahara et al., 1993; Gao et al., 2015, 2017; Li, Yang, et al., 2017; Sato et al., 1999, 2007).

Given the evidence of syntilting and posttilting overprints from the Lanping and Chuandian domains (as well as from the three sites in Triassic rocks from the Lanping domain), our data show that (1) The MT components always are prefolding, synfolding, and postfolding magnetization overprints; (2) ChRMs are overprinted in sites from the Simao (prefolding) and Chuandian (postfolding) domains, but a primary magnetization may be preserved in sites from Lanping domain edges that yield dual polarities; and (3) HT components yield dual-polarity prefolding directions and thus are similarly inferred to represent a primary remanence.

Our data are consistent with results of previous studies of red beds, showing that detrital hematite (or specularite) has high unblocking temperature spectra, clustered in the 600–660 °C to 680 °C temperature range, while fluid circulation and precipitation of newly formed hematite gives a CRM with a much broader laboratory unblocking temperature spectrum, from 200 to 680 °C (Jiang et al., 2015, 2017; Liu et al., 2011). We conclude that the MT components we find in demagnetization represent secondary CRMs, acquired both before and after folding, depending on the domain studied. In most cases, remagnetization completely erased any primary magnetization (ChRMs from the Simao and Chuandian domains), while in about 30% of the samples

(mostly from the Lanping domain) the primary remanence is preserved and was unblocked over 640–680 °C as the HT component. A similar dual polarity—presumably primary remanence unblocked in the 610–670 °C to 690 °C temperature range has been consistently reported from all domains of north Indochina (Chen et al., 1995; Huang & Opdyke, 1993; Kondo et al., 2012; Sato et al., 2001; Tanaka et al., 2008; Tong et al., 2013, 2015, 2016; Wang, Yang, et al., 2016; Yoshioka et al., 2003). Given this pattern, it is surprising that the ChRMs from Lanping domain edges seem to preserve a primary magnetization, implying that no CRM overprint occurred here.

Jiang et al. (2015) suggested that detrital hematite can be distinguished from secondary hematite arising from CRM, relying on the shape of thermal decay curves obtained during NRM demagnetization. In fact, CRM with a distributed unblocking temperature spectrum from ~200 to ~650 °C would yield concave shape thermal decay plots, while the confined spectrum from ~600 to ~680 °C of the depositional remanent magnetization would translate into convex demagnetization curves. Our data do not confirm this model (Figure 5), as nearly all thermal decay curves are convex in shape, regardless their dominant CRM, or the coexistence of a CRM and a depositional magnetization unblocked at 640–680 °C.

The question of the age of magnetization acquisition depends upon defining the age of folding, which is not well understood and is likely to have occurred over a long, late Oligocene to early Miocene (25–15 Ma), time span in our study area. Consequently, we are unable to assess whether a single CRM overprint event occurred in domains undergoing diachronous deformations or that diachronous CRM acquisition episodes took place in each of the domains examined. It is clear that magnetization overprinting was more pervasive in the Simao and Chuandian domains than in the sites in the Lanping area. Here, lateral domain boundaries seem to have escaped complete remagnetization, implying differences in the hydrothermal circulation pattern—responsible for CRM overprint—at domain center and in the vicinity of Chongshan and Ailao Shan-Red River shear zones.

3.3. Rotation Pattern and Crustal Block Size

Tilt-corrected data from the Simao domain show a nearly continuous spread of declinations from 3° to 81° (Figure 6) that is clearly suggestive of local block rotations. The pretilting remagnetization of those rocks implies that rotations should be evaluated considering Asian poles coeval to remagnetization age, instead of depositional ages. Considering the 25–15 Ma time span of folding, and the evidence that remagnetization occurred just prior to folding (e.g., Li, Yang, et al., 2017), we chose the 30 Ma Asia paleopole (Table 1) as a reference. Such choice is however not critical, as all post-130 Ma expected Asian declinations are $\leq$10° at north Indochina coordinates (Cogné et al., 2013), so that paleopole age errors would translate into $\leq$10° rotation errors. For site Yun52, rotations calculated from the (presumably primary) HT and MT components are statistically indistinguishable (57° $\pm$ 11° and 51° $\pm$ 12°, respectively).

The data from sites in the north Simao domain strikingly delineate six 2–5 km wide blocks (each defined by at least two adjacent sites with consistent rotation values) undergoing variable rotations (Figure 3a). From W to E, we identify three blocks that experienced 57° $\pm$ 9°, 48° $\pm$ 26, and 70° $\pm$ 1 CW rotations, separated by two unrotated blocks (sites Yun53-54 and Yun58-59). Finally, the two easternmost sites (Yun62-63) reveal a 23° $\pm$ 13° CW rotation.

Directions from the three sites in Triassic rocks from the Simao domain and sites from the Chuandian domain postdate tilting, so that rotations were calculated using the 20 Ma Asia pole and were based on in situ paleomagnetic directions. Rotation values are small (Figure 3), except for site Yun75 that is possibly an outlier (bedding orientation is completely different from that in nearby sites; Table 1). The posttilting rotations identified in the three Triassic sites (4° $\pm$ 11°), the three sites located just east the ARRSZ (−15° $\pm$ 16°) and the five sites located farther east (15° $\pm$ 14°) are at best barely significant, implying an overall absence of rotation of the ARRSZ and the Chuandian domain after magnetization acquisition (in turn postdating 25–15 Ma folding). Thus, our paleomagnetic data from the ARRSZ and the Chuandian domain are not relevant to understanding a rotation history, as we cannot exclude very recent age of remagnetization (i.e., within the last 0.78 Ma of the Brunhes polarity chron).

In the Lanping domain, large-magnitude rotations are observed at sites close to both the ARRSZ and the Chongshan shear zone (Figures 4 and 7). Rotations of three sites located adjacent to the ARRSZ may be of both senses, between 126° and 143°, and—as they approach 180°—their predominant CW or CCW sense

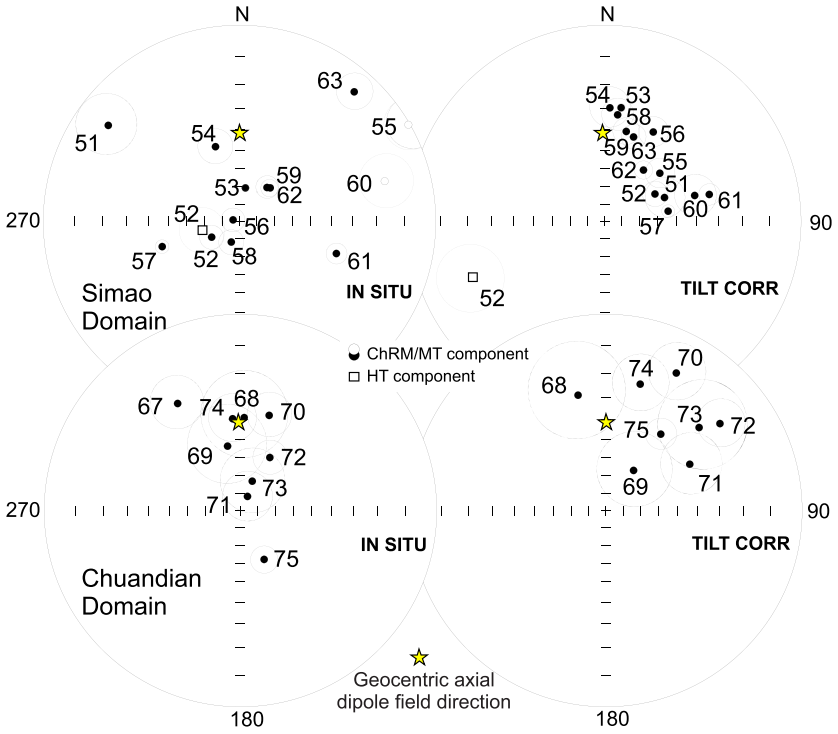

Figure 6. Equal-angle projections of estimated paleomagnetic directions obtained from Triassic-Cretaceous red beds exposed in the Simao and Chuandian domains. The three Triassic sites (Yun64-66) from the Simao domain are omitted. The yellow stars are the normal polarity geocentric axial dipole field direction ($D = 0°$; $I = 42°$) for the study area.

is obviously unclear. At the W Lanping domain margin, three sites located at 8–12 km distance from the Chongshan shear zone yield a 22–140° CCW rotation (the MT and HT components from site Yun82 give a 106° ± 13° and 140° ± 12° CCW rotation, respectively), and the adjacent Yun83 site gives a strikingly different 115° CW rotation. Conversely, HT components documented from Lanping domain center yield variable 37–95° CW rotations, apart for two sites just E of Yongping (Yun85-86), where a 27° ± 6° CCW rotation is estimated. MT components from the same sites show that these rocks experienced a remagnetization at 28% unfolding, and a subsequent lack of rotation (Figure 7). The occurrence of an unrotated—or barely CCW rotated—block just E of Yongping is confirmed by prefolding paleomagnetic directions reported by Funahara et al. (1993) and shown in Figure 4.

4. Discussion: Crust Fragmentation Within the Simao and Lanping "Blocks"

The highly rotated sites from the Lanping domain edges suggest that strike-slip deformation along the ARRSZ and Chongshan shear zones (constrained mainly at 32–15 Ma) resulted in the rotation of small kilometer size blocks up to a distance of at least 12 km from the shear zone (Figure 4). Such strike-slip-related crustal block rotations have been widely documented elsewhere (e.g., Beck, 1976; Hernandez-Moreno et al., 2014, 2016; Kimura et al., 2004, 2011; Piper et al., 1997; Randall et al., 2011; Ron et al., 1984). Within north Indochina, Pellegrino et al. (2018) showed that crust east of the Gaoligong shear zone was broken in ≥1 km wide crustal blocks that experienced CW rotations of about 180° and that rotations ended at a ~20 km distance from the shear zone. They suggested that rotation pattern is consistent with a quasi-continuous kinematic model (e.g., Sonder et al., 1994) and proposed a 230–290 km dextral offset for the Gaoligong shear zone based on rotation values and width of the block rotation zone.

Unfortunately, we cannot evaluate the block rotation pattern adjacent to shear zones, as only three sites are located adjacent (<5 km) to the ARRSZ. Therefore, the available paleomagnetic data are not useful to discriminate among the different estimates of the Oligo-Miocene ARRSZ offset (e.g., Leloup et al., 1995; Searle, 2006). We note—however—that the magnitude of the CCW rotation pattern indicated by sites located at

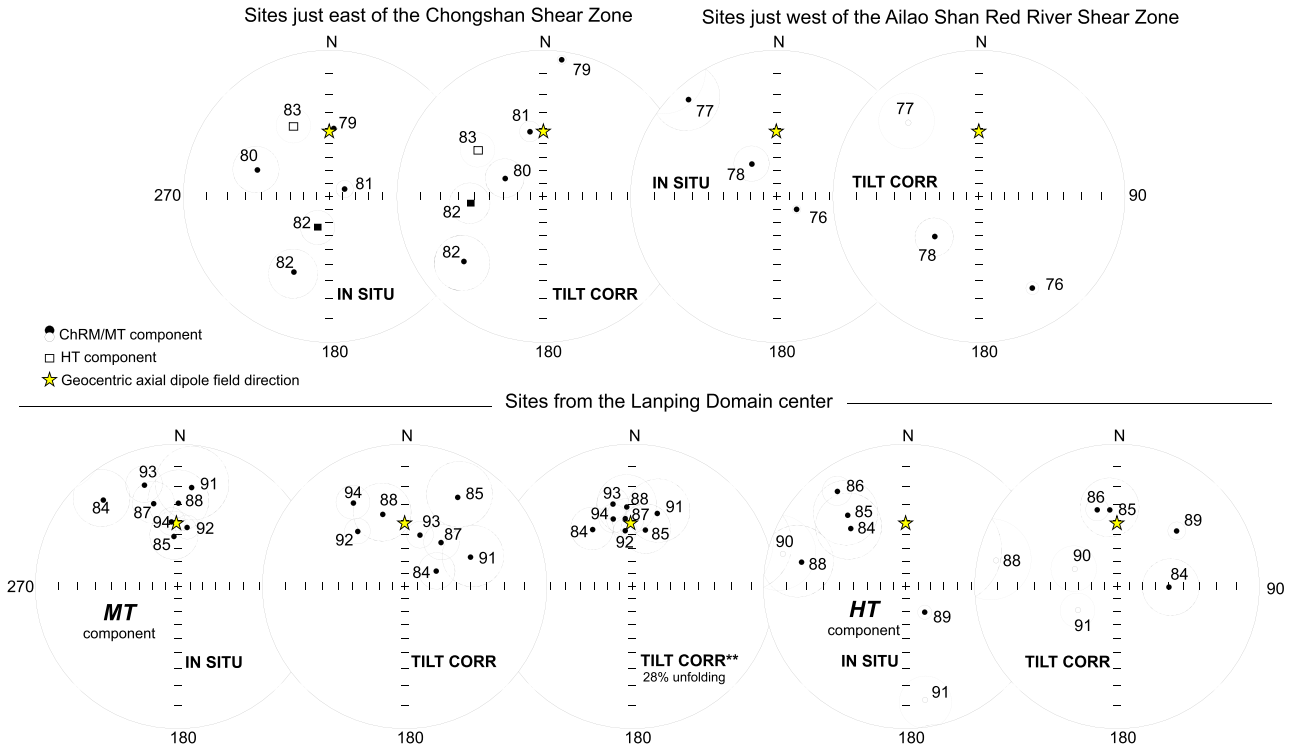

Figure 7. Equal-angle projections of the paleomagnetic directions obtained from Jurassic-Cretaceous red beds exposed in the Lanping domain. See text for explanation. The yellow stars are the normal polarity geocentric axial dipole field direction ($D = 0°$; $I = 44°$) for the study area.

8–12 km distance from the Chongshan shear zone is consistent with the left-lateral shear reported by Zhang et al. (2010) in the vicinity of our sampling sites, if both quasi-continuous (Sonder et al., 1994) and ball-bearing (Beck, 1976) crust deformation models are considered.

Paleomagnetic data from the internal part of the north Simao and Lanping "blocks" are interpreted to indicate internal "block" disruption into smaller semirigid subblocks (Figures 3a and 4). In the north Simao domain, three 2–5 km wide blocks that have rotated in a CW sense up to 70° are separated by two unrotated blocks. In the Lanping domain, CW rotations of variable (37–95°) magnitude are observed, although the data distribution is insufficient to define rotating block size. Moreover, data from two adjacent sites east of Yongping define an independent, 2–6 km wide block that suggests a 27° ± 6°CCW rotation. Similar evidence was consistently documented in the Lanping domain by both Funahara et al. (1993)—who studied several sites around Yongping (Figure 4)—and by Sato et al. (2001)—who reported results from Yunlong, ~50 km north of the location of our CCW rotated sites (Figure 2). Here, two Eocene red bed sites yield a reverse polarity and a null rotation, while other sites in the vicinity yield 60–100° CW rotations. Other areas from the Lanping domain that do not appear to have been rotated were also documented by Huang and Opdyke (1993) and Tanaka et al. (2008), although they are located adjacent to shear zones, thus possibly influenced by Chongshan and ARRSZ activity.

The small-scale block rotations identified in this study in the Lanping and Simao domains clearly indicate internal domain deformation that should be consistent with geologic evidence. Bedding orientations for the Lanping sampling sites show a considerable spread (Figure 8a) and are far from being predominantly NW in strike and subparallel to Chongshan and ARRSZ. Bedding orientation spreading is also apparent in the Simao domain (Figure 8b), although strikes trend mostly NW-SE—that is, subparallel to the ARRSZ. Bedding orientations are more constant along the N20°W trend in the Chuandian domain (apart from site Yun75; Figure 8c), while two sites closer to the ARRSZ have dispersed bedding attitudes.

Bedding orientation spreading observed at the Lanping and Simao domains suggests the possibility of polyphase deformation and/or local block rotations that are in fact documented by our paleomagnetic data. This is further support of the hypothesis that "block" interiors are far from being rigid and did not drift/rotate as a

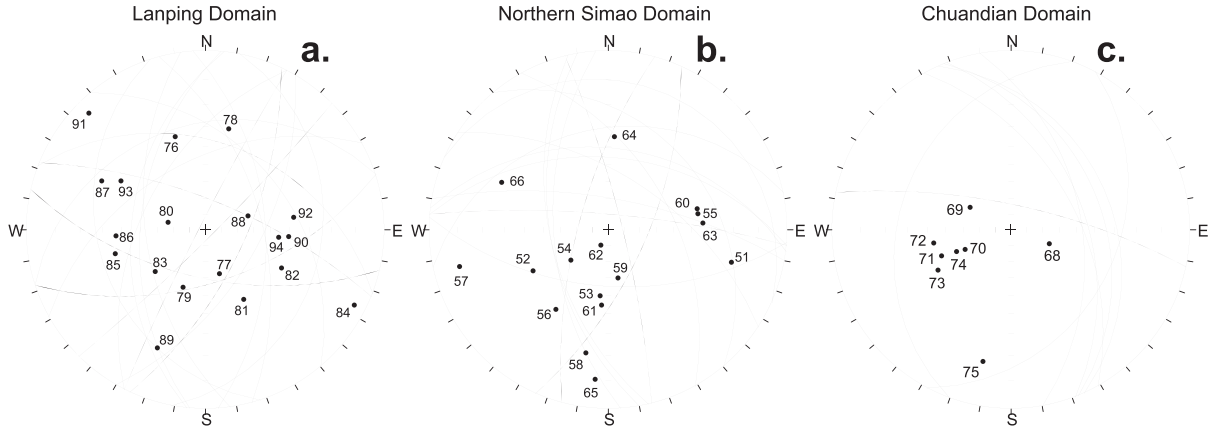

Figure 8. Equal-angle projections of bedding planes and normals to bedding at sampling sites from the (a) Lanping, (b) north Simao, and (c) Chuandian domain.

whole. Local rotations likely occurred along décollement at shallower depths than asthenosphere (where microplates are detached) and located in the lower ductile crust and/or along shallower thrust faults, as already proposed by Wang and Burchfiel (1997). Deformation is much more strong in the Lanping domain, where bedding orientations are nearly random (Figure 8a), suggesting a geological setting much more complex than that shown by available geological maps, which mainly document NW-SE oriented folds subparallel to the adjacent shear zones.

Crustal rotations that have taken place in deformed orogens have been either related to block rotation due to strike-slip shear (Hernandez-Moreno et al., 2014, and references therein) or to emplacement of rotational thrust sheets (e.g., Cifelli & Mattei, 2010; Shaanan et al., 2015; Speranza et al., 2018; Weil et al., 2010). Both kinematics are possible in the study area, as the Lanping and Simao domains are characterized by both strike-slip faults, and thrust structures (Bureau of Geology and Mineral Resources of Yunnan Province, 1990; Wang & Burchfiel, 1997). The small blocks delineated by our paleomagnetic results from the Simao domain are not always separated by faults according to maps of the Bureau of Geology and Mineral Resources of Yunnan Province, 1990 (Figure 3a), implying that other unrecognized structures are likely.

Similarly, a fault grid of unclear kinematics occurs in the Lanping domain, although some NW-SE trending thrust faults are apparent, mostly in the western domain zone (Figure 4). The two CCW rotated sites (Yun85-86) are not separated from the nearby CW rotated sites by any recognized structure. Thus, we are unable to provide a coherent tectonic model relating block rotations with thrust or strike-slip fault kinematics. Although this is not unexpected in an area heavily eroded and covered by extensive vegetation, we stress that more detailed geologic mapping and structural data from the Lanping and Simao domains are needed, hence to make better sense of models derived from paleomagnetic data. However, the considerable rotation consistency of couples of sites within a 2–5 km distance bounded by very differently rotated sites—as apparent in the Simao domain—strongly suggests an array of small semirigid rotating blocks bounded by strike-slip faults.

The internal deformation of the north Indochina "blocks" has been proposed in several papers, besides the seminal work by Wang & Burchfiel, 1997; Wang et al., 2008; Tanaka et al., 2008; Otofuji et al., 2012; Tsuchiyama et al., 2016). Other studies considered rotation variability to represent simply data scatter compared to megablock rigid rotations (Funahara et al., 1993; Huang & Opdyke, 1993, 2015; Li, Advokaat, et al., 2017; Li et al., 2018; Otofuji et al., 2010; Tong et al., 2016). Yoshioka et al. (2003), Kondo et al. (2012), and Gao et al. (2015) proposed that local rotations are due to oroclinal bending of already formed thrust-fold structures, a pattern that is not substantiated by our data.

It is not possible to assess by our data (or other data from the Lanping, Simao, and Baoshan domains) whether a uniform large-scale rotation is superimposed on the 2–5 km wide blocks that have independently rotated. The review by Li, Advokaat, et al. (2017) and data compiled in Figure 2 show that the whole Indochina (south of the Dien Bien Phu fault) and the Chuandian domain underwent a rather homogeneous Oligo-Miocene CW rotation of ~20°, whose tectonic cause is however beyond the scopes of this work.

4.1. Rotation Timing

Most of our sites are in Jurassic to Cretaceous age rocks and the data can be barely used to constrain the timing of rotation. However, assuming a 25–15 Ma magnetization overprint, a pulse of rotations from the north Simao and Lanping domain postdates and predates remagnetization, respectively (Figures 6 and 7).

Considering the evidence in the literature, Jurassic-Oligocene rocks from both the Simao and the Chuandian domain often show significant CW rotations, and remnants of Neogene sediments unconformably covering the older strata are essentially not rotated (Table S1 and Figure 2). Li, Yang, et al. (2017) reported data from Oligocene and mid-Miocene sedimentary rocks from the Jinggu area, about 100 km SW of our Simao study area (Figure 2). The Oligocene red beds were found to be remagnetized before tilting, then variably CW rotated in the 20–90° range, while gently dipping mid Miocene (ca. 15 Ma) sediments that may carry a primary magnetization were found to be nonrotated. Similar evidence was found in the same locality by Gao et al. (2015), who documented a CW rotation of ~70° in Cretaceous red beds, and only 10° of rotation in lower Miocene sandstones lying on older strata. Therefore, the whole process, including magnetization overprinting, rotation, and folding must be bracketed between ~25 Ma (late Oligocene age of the youngest rotated sediments) and ~15 Ma. Data from the Chuandian domain suggest a similar timing of these events, although CW rotations in Cretaceous-Oligocene red beds are rather constant around 20° (Figure 2), while upper Miocene (10–13 Ma) strata are not rotated (Li et al., 2015). Therefore, the CW rotation of the Chuandian domain is bracketed between about 25 and 13 Ma.

The synchronicity in time of remagnetization, rotation, and folding events within the 25–15 Ma age frame strongly suggests that such phenomena are genetically related. As suggested by Li, Yang, et al. (2017), it is likely that tectonism caused both fluid migration within fractured rock (thus chemical growth of pigmentary hematite) and rotations. Such an age window also overlaps with main age of strike-slip deformation documented along the major shear zones of Indochina (i.e., the Gaoligong, Chongshan, and ARRSZ, although onset of strike-slip shear is mostly set at a slightly older 32 Ma age; Leloup et al., 1993, 1995, 2001; Searle et al., 2010; Zhang et al., 2010; Zhang, Zhang, Chang, et al., 2012; Zhang, Zhang, Zhong, et al., 2012; Zhang et al., 2017).

It is noteworthy that block rotations in the Lanping domain (Figure 4) predated synfolding remagnetization, after which no further rotation occurred (Figure 7). This timing suggests a scenario where pristine rotating blocks bounded by secondary strike-slip faults within the Lanping domain caused subsequent tectonic deformation and folding of block margins, as well as related remanence overprinting due to fluid migration.

4.2. North Indochina Rotation Pattern due to Oblique Collision With Greater India NE Corner

Most authors explain the predominantly CW rotation pattern of north Indochina as related to the eastward extrusion of "microplates" during India-Eurasia collision (Funahara et al., 1993; Huang & Opdyke, 1993, 2015; Li, Advokaat, et al., 2017; Li et al., 2018; Otofuji et al., 2010; Tong et al., 2016). Our paleomagnetic data document upper crust fragmentation and independent deformation, including rotation, of 2–5 km wide blocks, instead of drifting/rotation of internally rigid lithospheric scale megablocks. Furthermore, paleomagnetic rotation timing (25–15 Ma) predates the circa 15 Ma onset of southeastward Tibet crust drift, clearly imaged at present by GPS data (Royden et al., 1997, 2008; Figure 1). Consequently, we suggest that tectonism of the "high-rotation corner," including the Baoshan, Lanping, and north Simao domains, was the consequence of oblique oceanic (both Neo-Tethys and Proto-Indian Ocean) subduction under Indochina, and eventual collision with the Greater India continental block (Figure 9).

According to paleogeographic reconstructions, subduction of the Neo-Tethys below Indochina dates back to at least mid-Jurassic times (ca. 160 Ma; e.g., Hall, 2012). Considering that the paleomargin trend was similar to the present-day one and that CW rotation of the whole Indochina does not exceed 20°, Li, Advokaat, et al., 2017, we hypothesize that a highly oblique subduction (~60°) occurred below Indochina for all of the Cenozoic. Subduction obliquity (defined as angle between normal to trench and convergence direction) can be approximated considering the trend of the India-Australia Transform fault—a requirement that follows from the India-Australia plate motions (e.g., Royer & Sandwell, 1989). This forms a small (30°) angle with the Indochina trench in early Cenozoic times. If a 20° CW rotation of the entirety of Indochina is considered, the prerotation subduction obliquity angle is reduced to ~40°.

Oblique strain in modern subduction zones is partitioned along pure dip-slip mega thrust faults, and strike-slip faults that usually bound fore-arc slivers drifting parallel to the trench (e.g. Beck, 1988; Dewey & Lamb, 1992). Present-day oblique subduction along the NE India margin is partitioned along pure dip-slip frontal thrust faults and dextral shear occurring along the Sagaing fault (Searle , 2006; Socquet & Pubellier, 2005; Figure 1).

We propose that after early-middle Cenozoic Neo-Tethys oblique subduction, the final docking of Greater India at the trench during the 32–15 Ma time span was partitioned by dextral shear along the Gaoligong fault (Figure 9) that was likely closer to the trench due to subsequent orogenic wedge enlargement and crustal slice accretion. Upper plate widening was enhanced farther south in Indonesia, as in this area subducting Indian Ocean plate rollback is documented after 20–15 Ma (Hall & Morley, 2004). Slab rollback has been shown to frequently induce drift and rotation of the upper plate (Shaanan et al., 2015; Speranza et al., 2002), thus potentially explaining the ~20° Oligo-Miocene CW rotation of the entire Indochina lithosphere documented by previous paleomagnetic data (e.g., Li, Advokaat, et al., 2017). Thermomechanical modeling data (Sternai et al., 2014) also confirm that slab rollback and the associated mantle return flow can modulate surface strain and drag the upper plate from below.

Considering an average 5 cm/year India-Indochina convergence (Molnar & Tapponnier, 1975), and an oblique 40° subduction/collision from 32 to 15 Ma (thus assuming to have occurred mostly before the 20° CW Indochina rotation) translates into a ~550 km plate-parallel dextral shear. This estimate is higher than the 230–290 km dextral displacement calculated by Pellegrino et al. (2018) for the Gaoligong fault on the basis of paleomagnetic data, implying that dextral shear parallel to the trench also occurred along other subparallel fault(s). After ~15 Ma, onset of southward crustal drift from Tibet changed the geodynamics of north Indochina, and dextral strain partitioning jumped farther west, along the Sagaing fault.

We suggest that at about 25–15 Ma the back-arc corner located between the Gaoligong and the ARRSZ was characterized by E-W shortening and that it fragmented into second-order strike-slip faults and 2–5 km size blocks, mostly rotating CW although also CCW rotation occurred (Figure 9). According to Zhang et al. (2010); Zhang, Zhang, Chang, et al., 2012; Zhang et al., 2017), paleoshortening directions along shear zones was approximately E-W during the early to mid Cenozoic (60–15 Ma), or ENE-WSW if a 20° CW rotation of the whole Indochina is considered. A shortening direction orthogonal to the trench is expected for a backarc independently from subduction obliquity, as presently observed east of the trench-parallel Liquiñe-Ofqui strike-slip fault of southern Chile (Orts et al., 2015).

A mid-Cenozoic E-W shortening direction implies that the paleo-Wanding, Nantinghe, and Dien Bien Phu faults (Figure 2) were possibly dextral in sense, and such kinematics—assuming quasi-continuous crust deformation models (e.g., Sonder et al., 1994)—could be the source for the widespread and large CW rotations observed in the Baoshan, Lanping, and Simao domains (Figure 9). Conversely, NW-SE faults would have been reactivated as sinistral faults, yielding CCW rotations, as the Chongshan shear zone segment located west of our CCW rotated sites from the Lanping domain (Figure 4; Zhang et al., 2010). We similarly suggest, following Wang and Burchfiel (1997) interpretation, that the ARRSZ was an inherited NW-SE crustal discontinuity that was reactivated with sinistral kinematics due to its favorable orientation with respect to E-W shortening. Thus, our data and model imply that the ARRSZ did not bound any major translating plate and thus was not a transform fault—as suggested by the extrusion block model of Tapponnier et al. (1990).

As E-W shortening in the Indochina dates back to 60–55 Ma (Zhang et al., 2010; Zhang et al., 2017; Zhang, Zhang, Chang, et al., 2012), the geodynamic change at 32 Ma that led to strike-slip activity along all shear zones was presumably due to docking of the Greater India NE corner at the Indochina trench. The timing of collision of Greater India with Asia is a highly debated issue, with recent syntheses placing it around 34 Ma (e.g., Aitchison et al., 2007). This age estimate is surprisingly similar to the onset of strike-slip deformation along major Indochina shear zones. The original shape of Greater India is unknown, and it is possible that its NE corner collided with Indochina around 32 Ma. Initially, major shear zones in Indochina bounded semi-rigid crustal blocks, but prolonged shear fragmented the blocks after 25 Ma, causing the formation of second-order strike-slip faults, resulting in small block rotations, remagnetization, and intense tectonic deformation.

The 25–15 Ma style of deformation has completely changed today (Figure 9). The southeastward drift of Tibet crust at a rate of ~2 cm/year (Liang et al., 2013; Figure 1) resulted in a N-S shortening that is clearly shown by focal mechanisms of predominant strike-slip earthquakes of magnitudes up to M of 7.0–7.5

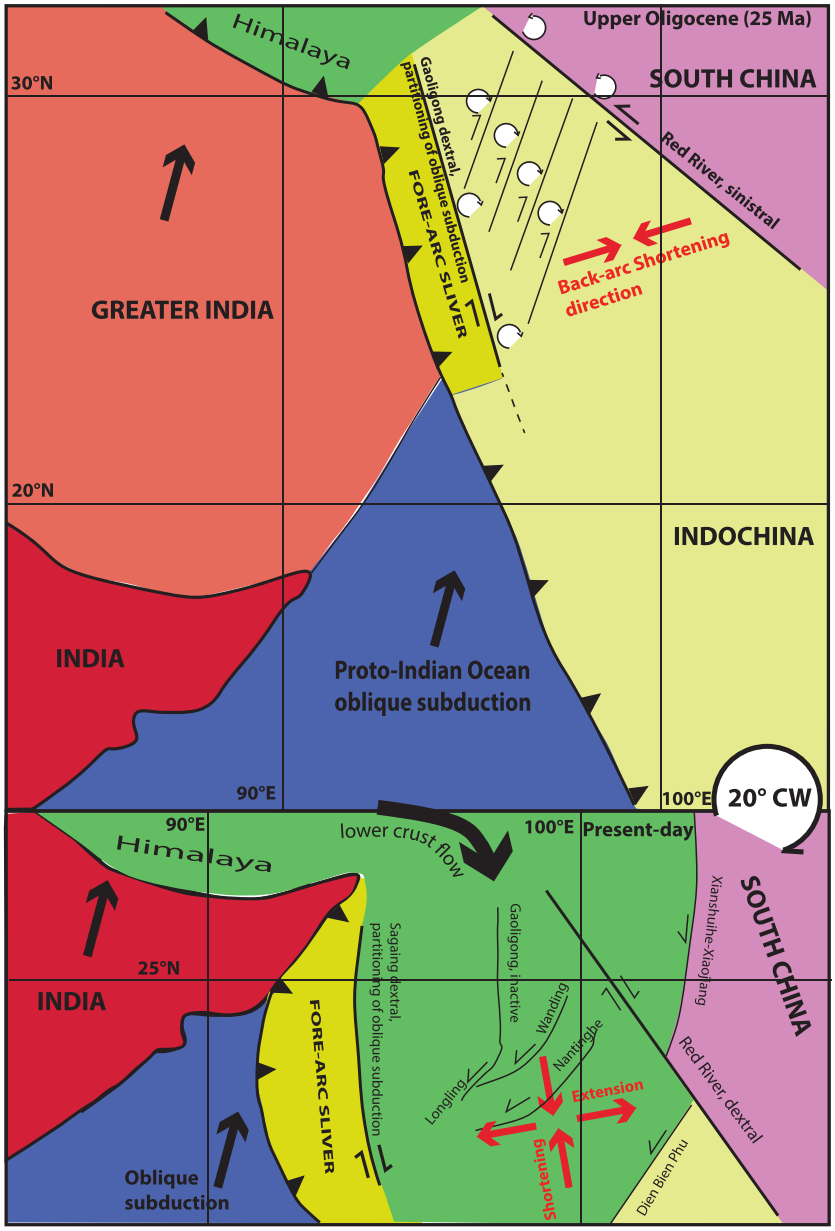

Figure 9. Paleogeographic reconstruction of Indochina and surrounding regions at 25 Ma (upper Oligocene), compared to the current setting. Yellow indicates parts of Indochina whose tectonism is the consequence of oblique sudduction of Proto-Indian Ocean and collision with Greater India. Green indicates Indochina sectors whose tectonics is influenced by southward flow of ductile lower crust from Tibet. Small circular arrows indicate small (1–5 km) block rotations that have taken place adjacent to strike-slip shear zones and within the Lanping and Simao domains at 25–15 Ma. All of Indochina experienced an ~20° semirigid CW rotation over the same time span (e.g., Li, Advokaat, et al., 2017) that is superimposed on the small block local rotations. Present-day shortening and extension directions (red arrows) are derived from GPS (Gan et al., 2007; Liang et al., 2013) and seismologic (Ekström et al., 2012) data.

(Ekström et al., 2012). N-S shortening is supposedly caused by the flow of ductile lower crust expanding from Tibet (Gan et al., 2007; Royden et al., 2008). The new stress regime has inverted the kinematics of strike-slip faults: the ARRSZ is currently dextral, the southern branch of the Gaoligong fault (called Longling fault) is sinistral, and yielded a M 7.4 strike-slip earthquake (Ekström et al., 2012). The Wanding, Nantinghe, and Dien Bien Phu faults are also sinistral at present, while the N-S branch of the Gaoligong fault, subparallel to the shortening direction, is consistently presently inactive.

5. Conclusions

New paleomagnetic data from north Indochina are interpreted to indicate that the northern Simao and Lanping "rigid drifting/rotating blocks" do not exist but comprise a mosaic of sub-blocks in the 2–5 km size order that experienced independent rotations. At both domain interiors, CW rotations of up to 95° dominate, but unrotated and slightly CCW rotated blocks also are defined by the data. Available geologic maps show, in both the Simao and Lanping domains, predominant NW-SE faults (mostly with reverse-slip kinematics) but do not reveal any tectonic features between many of the differently rotated blocks. Thus, a coherent model relating rotations and tectonics cannot be formulated at present. Further high-resolution geologic and structural investigations are required. However, the abrupt change of rotations magnitudes in adjacent sites is strongly suggestive of a small block rotation pattern driven by strike-slip faulting.

A complex process including hydrothermal fluid circulation and widespread remagnetization of Jurassic-Oligocene red beds, tectonic deformation (mainly strike-slip tectonics), and local block rotations occurred during the late Oligocene to mid Miocene, in the ~25–15 Ma time window. It is very likely that such processes—along with the 32–15 Ma phase of strike-slip ductile deformation in the major shear zones of north Indochina (Gaoligong, Chongshan, and ARRSZ)—were all genetically related. The small scale rotation of blocks is superimposed over a roughly synchronous large-scale ~20° CW rotation of the entire Indochina and Chuandian domain, which is well supported by all existing data (e.g., Li, Advokaat, et al., 2017), and is possibly related to the post-20 Ma rollback of the Indian Ocean slab below Indonesia (Hall & Morley, 2004).

The paleomagnetic documentation of small scale rotation of blocks, coupled with the proposed lower magnitude left-lateral displacement recently reevaluated for the ARRSZ (well below the originally proposed ~1,000 km; e.g., Searle, 2006, 2007), suggests that the tectonics of SE Asia was not characterized in Oligo-Miocene times by the eastward escape of semirigid microplates bounded by transform faults. Rather, it was a zone of diffuse crustal deformation, where 2–5 km size crustal blocks were rotated and detached above middle-lower crustal discontinuities, similarly to the crust kinematic model proposed by Wang and Burchfiel (1997).

The predominant CW rotation pattern of Indochina has been routinely related to lateral escape of Tibet crust, turning around the rigid buttress of NE Himalaya syntaxis. Yet, southward drift of crust from Tibet occurred in Indochina only after 15 Ma, when the paleomagnetic rotations were virtually over. Therefore, we suggest that block rotations occurred within a crust corner bounded by the Gaoligong and ARRSZ and subjected to intense E-W to ENE-WSW shortening, in the backarc of oblique collision of Greater India NE corner with Indochina. Data from the shear zones document an E-W shortening as old as 60–55 Ma, demonstrating the long-lasting influence of Neo-Tethys subduction within Indochina tectonics. We suggest that the change at 32–15 Ma characterized by tectonic deformation climax and strike-slip tectonics (and related paleomagnetic rotation) development was related to the arrival at trench of Greater India NE corner.

Strain partitioning of highly oblique Indochina-Greater India collision occurred at 32–15 Ma along the Gaoligong fault that—according to paleomagnetic data gathered at its vicinity—underwent a >200 km dextral shear. After 15 Ma, the locus of strain partitioning jumped west—accompanied by widening of the upper plate orogenic wedge—and occurs at present along the dextral Sagaing fault. We infer conversely that the sinistral shear along the ARRSZ was due to its NW orientation as a preexisting crustal discontinuity with respect to the Oligo-Miocene E-W shortening, consistently with Wang and Burchfiel (1997) who considered the ARRSZ an upper crustal transfer fault.

Acknowledgments
We are grateful to Mu for safely driving us over whole north Indochina. Thanks to Aldo Winkler for kindly solving a number of problems during lab measurements. This work was done in the frame of research projects funded by the National Key Research and Development Project of China (2016YFC0600303) and the National Science Foundation of China (NSFC) (41772207). A. G. P. and R. M. acknowledge a PhD and a "Chance" cod. 21040101 grant from Catania University, respectively. We are deeply indebted to Shihu Li, John Geissman, and an anonymous referee for providing careful reviews of our manuscript that helped to improve considerably our work. Thanks also to G-Cubed Associate Editor and Editor (Thorsten Becker) for carefully evaluating our paper. All paleomagnetic data supporting this work are available at institutional INGV FTP site address (ftp://ftp.ingv.it/pub/fabio.speranza/Data/).

References

Aitchison, J. C., Ali, J. R., & Davis, A. M. (2007). When and where did India and Asia collide? *Journal of Geophysical Research*, *112*, BO5423. https://doi.org/10.1029/2006JB004706

Akciz, S., Burchfiel, B. C., Crowley, J. L., Yin, J., & Chen, L. (2008). Geometry, kinematics, and regional significance of the Chong Shan shear zone, Eastern Himalayan Syntaxis. *Geosphere*, *4*(1), 292–314. https://doi.org/10.1130/GES00111.1

Beck, M. E. (1976). Discordant paleomagnetic pole positions as evidence of regional shear in the western Cordillera of North America. *American Journal of Science*, *276*, 694–712. https://doi.org/10.2475/ajs.276.6.694

Beck, M. E. (1988). Analysis of Late Jurassic-recent paleomagnetic data from active plate margins of South America. *The Journal of South American Earth Sciences*, *1*(1), 39–52. https://doi.org/10.1016/0895-9811(88)90014-4

Burchfiel, B. C., & Wang, E. (2003). Northwest-trending, middle Cenozoic, left-lateral faults in southern Yunnan, China, and their tectonic significance. *Journal of Structural Geology*, *25*(5), 781–792. https://doi.org/10.1016/S0191-8141(02)00065-2

Bureau of Geology and Mineral Resources of Xizang Autonomous Region (1993). *Regional geology of Xizang (Tibet) with 1/1,500,000 geological map (in Chinese with English abstract)*. Beijing: Geological Publishing House.

Bureau of Geology and Mineral Resources of Yunnan Province (1990). *Regional geology of Yunnan Province (in Chinese with English Abstract)*. Beijing: Geological Publishing House.

Chen, H., Dobson, J., Heller, F., & Hao, J. (1995). Paleomagnetic evidence for clockwise rotation of the Simao region since the Cretaceous: A consequence of India-Asia collision. *Earth and Planetary Science Letters*, *134*(1-2), 203–217. https://doi.org/10.1016/0012-821X(95)00118-V

Cifelli, F., & Mattei, M. (2010). Curved orogenic systems in the Italian peninsula: A paleomagnetic review. *Journal of the Virtual Explorer*, *36*, 17. https://doi.org/10.3809/jvirtex.2010.00239

Cogné, J. P., Besse, J., Chen, Y., & Hankard, F. (2013). A new Late Cretaceous to Present APWP for Asia and its implications for paleomagnetic shallow inclinations in Central Asia and Cenozoic Eurasian plate deformation. *Geophysical Journal International*, *192*(3), 1000–1024. https://doi.org/10.1093/gji/ggs104

Cohen, K. M., Finney, S. C., Gibbard, P. L., & Fan, J.-X. (2013). The ICSinternational chronostratigraphic chart. *Episodes*, *36*, 199–204.

Collinson, D. (1966). Carrier of remanent magnetization in certain red sandstones. *Nature*, *210*, 516–517.

Demarest, H. (1983). Error analysis for the determination of tectonic rotation from paleomagnetic data. *Journal of Geophysical Research*, *88*(B5), 4321–4328. https://doi.org/10.1029/JB088iB05p04321

Dewey, J. F., & Lamb, S. H. (1992). Active tectonics of the Andes. *Tectonophysics*, *205*(1–3), 79–95. https://doi.org/10.1016/0040-1951(92)90419-7

Ekström, G., Nettles, M., & Dziewonski, A. M. (2012). The global CMT project 2004-2010: Centroid-moment tensors for 13,017 earthquakes. *Physics of the Earth and Planetary Interiors*, *200-201*, 1–9. https://doi.org/10.1016/j.pepi.2012.04.002

Fisher, R. A. (1953). Dispersion on a sphere. *Proceedings of the Royal Society A*, *217*, 295–305. https://doi.org/10.1098/rspa.1953.0064

Funahara, S., Nishiwaki, N., Miki, M., Murata, F., Otofuji, Y., & Wang, Y. Z. (1992). Paleomagnetic study of Cretaceous rocks from the Yangtze block, central Yunnan, China: Implications for the India-Asia collision. *Earth and Planetary Science Letters*, *113*(1-2), 77–91. https://doi.org/10.1016/0012-821X(92)90212-E

Funahara, S., Nishiwaki, N., Murata, F., Otofuji, Y., & Wang, Y. Z. (1993). Clockwise rotation of the Red River fault inferred from paleomagnetic study of Cretaceous rocks in the Shan-Thai-Malay Block of western Yunnan, China. *Earth and Planetary Science Letters*, *117*(1-2), 29–42. https://doi.org/10.1016/0012-821X(93)90115-P

Gan, W. J., Zhang, P. Z., Shen, Z. K., Niu, Z. J., Wang, M., Wan, Y. G., et al. (2007). Present-day crustal motion within the Tibetan Plateau inferred from GPS measurements. *Journal of Geophysical Research*, *112*, B08416. https://doi.org/10.1029/2005JB004120

Gao, L., Yang, Z., Tong, Y., Wang, H., & An, C. (2015). New paleomagnetic studies of Cretaceous and Miocene rocks from Jinggu, western Yunnan, China: Evidence for internal deformation of the Lanping–Simao Terrane. *Journal of Geodynamics*, *89*, 39–59. https://doi.org/10.1016/j.jog.2015.06.004

Gao, L., Yang, Z., Tong, Y., Wang, H., An, C., & Zhang, H. (2017). Cenozoic clockwise rotation of the Chuan Dian Fragment, southeastern edge of the Tibetan Plateau: Evidence from a new paleomagnetic study. *Journal of Geodynamics*, *112*, 46–57. https://doi.org/10.1016/j.jog.2017.10.001

Gradstein, F. M., Ogg, J. G., Schmitz, M. D., & Ogg, G. M. (2012). *The geologic time scale* (Vol. 1176). Amsterdam: Elsevier. https://doi.org/10.1016/C2011-1-08249-8

Hall, R. (2012). Late Jurassic-Cenozoic reconstructions of the Indonesian region and the Indian Ocean. *Tectonophysics*, *570-571*, 1–41. https://doi.org/10.1016/j.tecto.2012.04.021

Hall, R., & Morley, C. K. (2004). Sundaland basins. In P. Clift, W. Wang, & H. Kuhnt (Eds.), *Continent-Ocean Interactions within the East Asian Marginal Seas Geophysical Monograph* (Vol. 149, pp. 55–85). Washington, DC: American Geophysical Union.

He, K., He, H., & Cai, H. (1996). Formation and evolution of the western Yunnan orogenic belt. *Geological Review*, *42*(2), 97–106.

Hernandez-Moreno, C., Speranza, F., & Di Chiara, A. (2014). Understanding kinematics of intra-arc transcurrent deformation: Paleomagnetic evidence from the Liquiñe-Ofqui fault zone (Chile, 38–41°S). *Tectonics*, *33*, 1964–1988. https://doi.org/10.1002/2014TC003622

Hernandez-Moreno, C., Speranza, F., & Di Chiara, A. (2016). Paleomagnetic rotation pattern of the southern Chile fore-arc sliver (38°S–42°S): A new tool to evaluate plate locking along subduction zones. *Journal of Geophysical Research: Solid Earth*, *121*, 469–490. https://doi.org/10.1002/2015JB012382

Houseman, G., & England, P. (1986). Finite strain calculations of continental deformation 1.Method and general results for convergent ones. *Journal of Geophysical Research*, *91*(B3), 3651–3663. https://doi.org/10.1029/JB091iB03p03651

Houseman, G., & England, P. (1993). Crustal thickening versus lateral expulsion in the Indian-Asian continental collision. *Journal of Geophysical Research*, *98*(B7), 12,233–12,249. https://doi.org/10.1029/93JB00443

Huang, K., & Opdyke, N. D. (1993). Paleomagnetic results from Cretaceous and Jurassic rocks of South and Southwest Yunnan: Evidence for large clockwise rotations in the Indochina and Shan-Thai-Malay terranes. *Earth and Planetary Science Letters*, *117*(3-4), 507–524. https://doi.org/10.1016/0012-821X(93)90100-N

Huang, K., & Opdyke, N. D. (2015). Post-folding magnetization of the Triassic rocks from western Guizhou and southern Yunnan provinces: New evidence for large clockwise rotations in the Simao Terrane. *Earth and Planetary Science Letters*, *423*, 155–163. https://doi.org/10.1016/j.epsl.2015.05.015

Huang, Z., Tilmann, F., Xu, M., Wang, L., Ding, Z., Mi, N., et al. (2017). Insight into NE Tibetan Plateau expansion from crustal and upper mantle anisotropy revealed by shear-wave splitting. *Earth and Planetary Science Letters*, *478*, 66–75. https://doi.org/10.1016/j.epsl.2017.08.030

Jiang, Z., Liu, Q., Dekkers, M. J., Tauxe, L., Qin, H., Barrón, V., & Torrent, J. (2015). Acquisition of chemical remanent magnetization during experimental ferrihydrite-hematite conversion in Earth-like magnetic field-implications for paleomagnetic studies of red beds. *Earth and Planetary Science Letters*, *428*, 1–10. https://doi.org/10.1016/j.epsl.2015.07.024

Jiang, Z., Liu, Q., Dekkers, M. J., Zhao, X., Roberts, A. P., Yang, Z., et al. (2017). Remagnetization mechanisms in Triassic red beds from South China. *Earth and Planetary Science Letters*, *479*, 219–230. https://doi.org/10.1016/j.epsl.2017.09.019

Kent, D. V., Xu, G., Huang, K., Zhang, W., & Opdyke, N. D. (1986). Paleomagnetism of upper Cretaceous rocks from South China. *Earth and Planetary Science Letters*, *79*(1), 179–184.

Kimura, H., Ishikawa, N., & Sato, H. (2011). Estimation of total lateral displacement including strike-slip offset and broader drag deformation on an active fault: Tectonic geomorphic and paleomagnetic evidence on the Tanna fault zone in central Japan. *Tectonophysics*, *501*(1–4), 87–97. https://doi.org/10.1016/j.tecto.2011.01.016

Kimura, H., Itoh, Y., & Tsutsumi, H. (2004). Quaternary strike-slip crustal deformation around an active fault based on paleomagnetic analysis: A case study of the Enako fault in central Japan. *Earth and Planetary Science Letters*, *226*(3–4), 321–334. https://doi.org/10.1016/j.epsl.2004.08.003

Kirschvink, J. L. (1980). The least-squares line and plane and the analysis of paleomagnetic data. *Geophysics Journal International*, *62*(3), 699–718. https://doi.org/10.1111/j.1365-246X.1980.tb02601.x

Kondo, K., Mu, C., Yamamoto, T., Zaman, H., Miura, D., Yokoyama, M., et al. (2012). Oroclinal origin of the Simao Arc in the Shan-Thai Block inferred from the Cretaceous paleomagnetic data. *Geophysical Journal International*, *190*(1), 201–216. https://doi.org/10.1111/j.1365-246X.2012.05467.x

Kornfeld, D., Eckert, S., Appel, E., Ratschbacher, L., Pfänder, J., Liu, D., & Ding, L. (2014a). Clockwise rotation of the Baoshan block due to southeastward tectonic escape of Tibetan crust since the Oligocene. *Geophysical Journal International*, *197*(1), 149–163. https://doi.org/10.1093/gji/ggu009

Kornfeld, D., Eckert, S., Appel, E., Ratschbacher, L., Sonntag, B.-L., Pfänder, J. A., et al. (2014b). Cenozoic clockwise rotation of the Tengchong block, southeastern Tibetan Plateau: A paleomagnetic and geochronologic study. *Tectonophysics*, *628*, 105–122. https://doi.org/10.1016/j.tecto.2014.04.032

Leloup, P. H., Harrison, T. M., Ryerson, F. J., Wenji, C., Qi, L., Tapponnier, P., & Lacassin, R. (1993). Structural, petrological and thermal evolution of a Tertiary ductile strike-slip shear zone, Diancang Shan, Yunnan. *Journal of Geophysical Research*, *98*(B4). https://doi.org/10.1029/92JB02791

Leloup, P. H., Lacassin, R., Tapponnier, P., & Harrison, T. M. (2001). Comment on "Onset timing of left-lateral movement along the Ailao Shan-Red river shear zone: Ar-40/Ar-39 dating constraint from the Nam Dinh area, northeastern Vietnam" by Wang et al., 2000. Journal of Asian Earth Sciences 18, 281–292. *Journal of Asian Earth Sciences*, *20*(1), 95–99. https://doi.org/10.1016/S1367-9120(01)00034-7

Leloup, P. H., Lacassin, R., Tapponnier, P., Scharer, U., Zhong, D., Liu, X., et al. (1995). The Ailao Shan-Red River shear zone (Yunnan, China), Tertiary transform boundary of Indochina. *Tectonophysics*, *251*(1-4), 3–10. https://doi.org/10.1016/0040-1951(95)00070-4

Leloup, P. H., Tapponnier, P., & Lacassin, R. (2007). Discussion on the role of the Red River shear zone, Yunnan and Vietnam, in the continental extrusion of SE Asia. *Journal of the Geological Society*, *164*, 1253–1260. https://doi.org/10.1144/0016-76492007-065

Li, S., Advokaat, E. L., Van Hinsbergen, D. J. J., Koymans, M., Deng, C., & Zhu, R. (2017). Paleomagnetic constraints on the Mesozoic-Cenozoic paleolatitudinal and rotational history of Indochina and South China: Review and updated kinematic reconstruction. *Earth-Science Reviews*, *171*, 58–77. https://doi.org/10.1016/j.earscirev.2017.05.007

Li, S., Deng, C., Dong, W., Sun, L., Liu, S., Qin, H., et al. (2015). Magnetostratigraphy of the Xiaolongtan Formation bearing *Lufengpithecus keiyuanensis* in Yunnan, southwestern China: Constraint on the initiation time of the southern segment of the Xianshuihe-Xiaojiang fault. *Tectonophysics*, *655*, 213–226. https://doi.org/10.1016/j.tecto.2015.06.002

Li, S., Deng, C., Yao, H., Huang, S., Liu, C., He, H., et al. (2013). Magnetostratigraphy of the Dali Basin in Yunnan and implications for late Neogene rotation of the southeast margin of the Tibetan Plateau. *Journal of Geophysical Research: Solid Earth*, *118*, 791–807. https://doi.org/10.1002/jgrb.50129

Li, S., Van Hinsbergen, D. J. J., Deng, C., Advokaat, E. L., & Zhu, R. (2018). Paleomagnetic constraints from the Baoshan area on the deformation of the Qiangtang-Sibumasu Terrane around the eastern Himalayan syntaxis. *Journal of Geophysical Research: Solid Earth*, *123*, 977–997. https://doi.org/10.1002/2017JB015112

Li, S., Yang, Z., Deng, C., He, H., Qin, H., Sun, L., et al. (2017). Clockwise rotations recorded in redbeds from the Jinggu Basin of northwestern Indochina. *Geological Society of America Bulletin*, *129*(9-10), 1100–1122. https://doi.org/10.1130/B31637.1

Liang, S., Gan, W., Shen, C., Xiao, G., Liu, J., Chen, W., et al. (2013). Three-dimensional velocity field of present-day crustal motion of the Tibetan Plateau derived from GPS measurements. *Journal of Geophysical Research: Solid Earth*, *118*, 5722–5732. https://doi.org/10.1002/2013JB010503

Liu, C., Ge, K., Zhang, C., Liu, Q., Deng, C., & Zhu, R. (2011). Nature of remagnetization of Lower Triassic red beds in southwestern China. *Geophysical Journal International*, *187*(3), 1237–1249. https://doi.org/10.1111/j.1365-246X.2011.05196.x

Lowrie, W. (1990). Indentification of Ferromagnetic minerals in a rock by coercivity and unblocking temperature properties. *Geophysical Research Letters*, *17*(2), 159–162. https://doi.org/10.1029/GL017i002p00159

McFadden, P. L. (1990). A new fold test for paleomagnetic studies. *Geophysical Journal International*, *103*(1), 163–169. https://doi.org/10.1111/j.1365-246X.1990.tb01761.x

McKenzie, D., & Jackson, J. (1986). A block model of distributed deformation by faulting. *Journal of Geological Society*, *143*(2), 349–353. https://doi.org/10.1144/gsjgs.143.2.0349

Meade, B. J. (2007). Present-day kinematics at the India-Asia collision zone. *Geology*, *35*(1), 81–84. https://doi.org/10.1130/G22924A.1

Meng, Q. R., & Zhang, G. W. (1999). Timing of collision of the North and South China blocks: controversy and reconciliation. *Geology*, *27*(2), 123–126. https://doi.org/10.1130/0091-7613(1999)027<0123:TOCOTN>2.3.CO;2

Molnar, P., Fitch, T. J., & Wu, F. T. (1973). Fault plane solution of shallow earthquakes and contemporary tectonics in Asia. *Earth and Planetary Science Letters*, *19*(2), 101–112. https://doi.org/10.1016/0012-821X(73)90104-0

Molnar, P., & Tapponnier, P. (1975). Cenozoic tectonics of Asia: effects of a continental collision. *Science*, *189*(4201), 419–426. https://doi.org/10.1126/science.189.4201.419

Nelson, K. D., Zhao, W. J., Brown, L. D., Kuo, J., Che, J. K., Liu, X. W., et al. (1996). Partially molten middle crust beneath southern Tibet: Synthesis of Project INDEPTH Results. *Science*, *174*(5293), 1684–1688. https://doi.org/10.1126/science.274.5293.1684

Nelson, M. R., & Jones, C. H. (1987). Paleomagnetism and crustal rotations along a shear zone, Las Vegas Range, southern Nevada. *Tectonics*, *6*(1), 13–33. https://doi.org/10.1029/TC006i001p00013

Orts, D. L., Folguera, A., Giménez, M., Ruiz, F., Rojas, V. E. A., & Lince Klinger, F. (2015). Cenozoic building and deformational processes in the North Patagonian Andes. *Journal of Geodynamics*, *86*, 26–41. https://doi.org/10.1016/j.jog.2015.02.002

Otofuji, Y., Liu, Y., Yokoyama, M., Tamai, M., & Yin, J. (1998). Tectonic deformation of the southwestern part of the Yangtze craton inferred from paleomagnetism. *Earth and Planetary Science Letters*, *156*(1-2), 47–60. https://doi.org/10.1016/S0012-821X(98)00009-0

Otofuji, Y., Tung, V. D., Fujihara, M., Tanaka, M., Yokoyama, M., Kitada, K., & Zaman, H. (2012). Tectonic deformation of the southeastern tip of the Indochina Peninsula during its southward displacement in the Cenozoic time. *Gondwana Research*, *22*(2), 615–627. https://doi.org/10.1016/j.gr.2011.09.015

Otofuji, Y., Yokoyama, M., Kitada, K., & Zaman, H. (2010). Paleomagnetic versus GPS determined tectonic rotation around eastern Himalayan Syntaxis in East Asia. *Journal of Asian Earth Sciences*, *37*(5-6), 438–451. https://doi.org/10.1016/j.jseaes.2009.11.003

Pellegrino, A. G., Zhang, B., Speranza, F., Maniscalco, R., Yin, C., Hernandez-Moreno, C., & Winkler, A. (2018). Tectonics and paleomagnetic rotation pattern of Yunnan (24°N–25°N, China): Gaoligong fault shear versus megablock drift. *Tectonics*, *37*, 1524–1551. https://doi.org/10.1029/2017TC004899

Piper, J. D. A., Tatar, O., & Gürsoy, H. (1997). Deformational behavior of continental lithosphere deduced from block rotations across the North Anatolian Fault Zone in Turkey. *Earth and Planetary Science Letters*, *150*(3-4), 191–203. https://doi.org/10.1016/S0012-821X(97)00103-9

Randall, K., Lamb, S., & Mac Niocaill, C. (2011). Large tectonic rotations in a wide zone of Neogene distributed dextral shear, northeastern South Island, New Zealand. *Tectonophysics*, *509*(3-4), 165–180. https://doi.org/10.1016/j.tecto.2011.05.006

Ron, H., Freund, R., Garfunkel, Z., & Nur, A. (1984). Block rotation by strike-slip faulting: Structural and paleomagnetic evidence. *Journal of Geophysical Research*, *89*(B7), 6256–6270. https://doi.org/10.1029/JB089iB07p06256

Royden, L. H., Burchfiel, B. C., King, R., Wang, E., Chen, Z., Shen, F., & Liu, Y. (1997). Surface deformation and lower crustal flow in Eastern Tibet. *Science*, *276*(5313), 788–790. https://doi.org/10.1126/science.276.5313.788

Royden, L. H., Burchfiel, B. C., & Van der Hilst, R. D. (2008). The geological evolution of the Tibetan Plateau. *Science*, *321*(5892), 1054–1058. https://doi.org/10.1126/science.1155371

Royer, J.-Y., & Sandwell, D. T. (1989). Evolution of the eastern Indian Ocean since the Late Cretaceous: Constraints from GEOSAT altimetry. *Journal of Geophysical Research*, *94*(B10), 13,755–13,782. https://doi.org/10.1029/JB094iB10p13755

Sato, K., Liu, Y., Wang, Y., Yokoyama, M., Yoshioka, S., Yang, Z., & Otofuji, Y. (2007). Paleomagnetic study of Cretaceous rocks from Pu'er, western Yunnan, China: Evidence of internal deformation of the Indochina Block. *Earth and Planetary Science Letters*, *258*(1-2), 1–15. https://doi.org/10.1016/j.epsl.2007.02.043

Sato, K., Liu, Y., Zhu, Z., Yang, Z., & Otofuji, Y. (1999). Paleomagnetic study of middle Cretaceous rocks from Yunlong, western Yunnan, China: Evidence of south-ward displacement of Indochina. *Earth and Planetary Science Letters*, *165*(1), 1–15. https://doi.org/10.1016/S0012-821X(98)00257-X

Sato, K., Liu, Y., Zhu, Z., Yang, Z., & Otofuji, Y. (2001). Tertiary paleomagnetic data from northwestern Yunnan, China: Further evidence for large clockwise rotation of the Indochina Block and its tectonic implications. *Earth and Planetary Science Letters*, *185*(1-2), 185–198. https://doi.org/10.1016/S0012-821X(00)00377-0

Schoenbohm, L., Burchfiel, B. C., Chen, L., & Yin, J. (2006). Miocene to present activity along the Red River fault, China, in the context of continental extrusion, upper-crustal rotation, and lower-crustal flow. *Geological Society of America Bulletin*, *118*(5-6), 672–688. https://doi.org/10.1130/B25816.1

Searle, M. (2007). Discussion on the role of the Red River shear zone, Yunnan and Vietnam, in the continental extrusion of SE Asia—Reply. *Journal of the Geological Society*, *164*, 1253–1260.

Searle, M. P. (2006). Role of the Red River Shear zone, Yunnan and Vietnam, in the continental extrusion of SE Asia. *Journal of the Geological Society*, *163*(6), 1025–1036. https://doi.org/10.1144/0016-76492005-144

Searle, M. P., Yeh, M. W., Lin, T. H., & Chung, S. L. (2010). Structural constraints on the timing of left-lateral shear along the Red River shear zone in the Ailao Shan and Diancang Shan Ranges, Yunnan, SW China. *Geosphere*, *6*(4), 316–338. https://doi.org/10.1130/GES00580.1

Shaanan, U., Rosenbaum, G., Pisarevsky, S., & Speranza, F. (2015). Paleomagnetic data from the New England Orogen (eastern Australia) and implications for oroclinal bending. *Tectonophysics*, *664*, 182–190. https://doi.org/10.1016/j.tecto.2015.09.018

Socquet, A., & Pubellier, M. (2005). Cenozoic deformation in western Yunnan (China–Myanmar border). *Journal of Asian Earth Sciences*, *24*(4), 495–515. https://doi.org/10.1016/j.jseaes.2004.03.006

Sonder, L. J., Jones, C. H., Salyards, S. L., & Murphy, K. M. (1994). Vertical axis rotations in the Las Vegas Valley Shear Zone, southern Nevada: Paleomagnetic constraints on kinematics and dynamics of block rotations. *Tectonics*, *13*(4), 769–788. https://doi.org/10.1029/94TC00352

Speranza, F., Hernandez-Moreno, C., Avellone, G., Morticelli, M. G., Agate, M., Sulli, A., & Di Stefano, E. (2018). Understanding Paleomagnetic rotations in Sicily: Thrust versus strike-slip tectonics. *Tectonics*, *37*, 1138–1158. https://doi.org/10.1002/2017TC004815

Speranza, F., Villa, I. M., Sagnotti, L., Florindo, F., Cosentino, D., Cipollari, P., & Mattei, M. (2002). Age of the Corsica-Sardinia rotation and Liguro-Provencal Basin spreading: New paleomagnetic and Ar/Ar evidence. *Tectonophysics*, *347*, 231–251.

Sternai, P., Jolivet, L., Menant, A., & Gerya, T. (2014). Driving the upper plate surface deformation by slab rollback and mantle flow. *Earth and Planetary Science Letters*, *405*, 110–118. https://doi.org/10.1016/j.epsl.2014.08.023

Tanaka, K., Mu, C., Sato, K., Takemoto, K., Miura, D., Liu, Y., et al. (2008). Tectonic deformation around the eastern Himalayan Syntaxis: Constraints from the Cretaceous palaeomagnetic data of the Shan-Thai Block. *Geophysical Journal International*, *175*(2), 713–728. https://doi.org/10.1111/j.1365-246X.2008.03885.x

Tapponnier, P., Lacassin, R., Leloup, P. H., Schärer, U., Zhong, D., Wu, H., et al. (1990). The Ailao Shan–Red River Metamorphic belt: Tertiary left lateral shear between Indochina and South China. *Nature*, *343*, 431–437. https://doi.org/10.1038/343431a0

Tapponnier, P., & Molnar, P. (1977). Active faulting and tectonics in China. *Journal of Geophysical Research*, *82*(20), 2905–2930. https://doi.org/10.1029/JB082i020p02905

Tapponnier, P., Peltzer, G., Le Dain, A. Y., Armijo, R., & Cobbold, P. (1982). Propagating extrusion tectonics in Asia: New insights from simple experiments with plasticine. *Geology*, *10*(12), 611–616. https://doi.org/10.1130/0091-7613(1982)10<611:PETIAN>2.0.CO;2

Tong, Y.-B., Yang, Z., Gao, L., Wang, H., Zhang, X.-D., An, C.-Z., et al. (2015). Paleomagnetism of Upper Cretaceous red-beds from the eastern Qiangtang Block: Clockwise rotations and latitudinal translation during the India–Asia collision. *Journal of Asian Earth Sciences*, *114*(4), 732–749. https://doi.org/10.1016/j.jseaes.2015.08.016

Tong, Y.-B., Yang, Z., Jing, X., Zhao, Y., Li, C., Huang, D., & Zhang, X. (2016). New insights into the Cenozoic lateral extrusion of crustal blocks on the southeastern edge of Tibetan Plateau: Evidence from paleomagnetic results from Paleogene sedimentary strata of the Baoshan Terrane. *Tectonics*, *35*, 2494–2514. https://doi.org/10.1002/2016TC004221

Tong, Y.-B., Yang, Z., Mao, C., Pei, J., Pu, Z., & Xu, Y. (2017). Paleomagnetism of Eocene red-beds in the eastern part of the Qiangtang Terrane and its implications for uplift and southward crustal extrusion in the southeastern edge of the Tibetan Plateau. *Earth and Planetary Science Letters*, *475*, 1–14. https://doi.org/10.1016/j.epsl.2017.07.026

Tong, Y.-B., Yang, Z., Zheng, L. D., Xu, Y. L., Wang, H., Gao, L., & Hu, X. Z. (2013). Internal crustal deformation in the northern part of Shan-Thai Block: New evidence from paleomagnetic results of Cretaceous and Paleogene redbeds. *Tectonophysics*, *608*, 1138–1158. https://doi.org/10.1016/j.tecto.2013.06.031

Torsvik, T. H., van der Voo, R., Preeden, U., Mac Niocaill, C., Steinberger, B., Doubrovine, P. V., et al. (2012). Phanerozoic polar wander, paleogeography and dynamics. *Earth-Science Reviews*, *114*(3-4), 325-368. https://doi.org/10.1016/j.earscirev.2012.06.007

Tsuchiyama, Y., Zaman, H., Sotham, S., Samuth, Y., Sato, E., Ahn, H.-S., et al. (2016). Paleomagnetism of Late Jurassic to Early Cretaceous red beds from the Cardamom Mountains, southwestern Cambodia: Tectonic deformation of the Indochina Peninsula. *Earth and Planetary Science Letters*, *434*, 274–288. https://doi.org/10.1016/j.epsl.2015.11.045

Walker, T. R., Larson, E. E., & Hoblitt, R. P. (1981). Nature and origin of hematite in the Moenkopi Formation (Triassic), Colorado Plateau: A contribution to the origin of magnetism in red beds. *Journal of Geophysical Research*, *86*(B1), 317–333. https://doi.org/10.1029/JB086iB01p00317

Wang, E., & Burchfiel, B. C. (1997). Interpretation of Cenozoic tectonics in the right-lateral accommodation zone between the Ailao Shan shear zone and the Eastern Himalayan Syntaxis. *International Geology Review*, *39*, 191–219. https://doi.org/10.1080/00206819709465267

Wang, E., Burchfiel, B. C., Royden, L. H., Chen, L. Z., Chen, J. S., Li, W. X., & Chen, Z. L. (1998). Late Cenozoic Xianshuihe–Xiaojiang, Red River, and Dali Fault Systems of Southwestern Sichuan and Central Yunnan, China. *Geological Society of America Special Papers*, *327*, 1–108. https://doi.org/10.1130/0-8137-2327-2.1

Wang, G., Wan, J., Wang, E., Zheng, D., & Li, F. (2008). Late Cenozoic to recent transtensional deformation across the Southern part of the Gaoligong shear zone between the Indian plate and SE margin of the Tibetan plateau and its tectonic origin. *Tectonophysics*, *460*(1-4), 1–20. https://doi.org/10.1016/j.tecto.2008.04.007

Wang, H., Yang, Z., Tong, Y., Gao, L., Jing, X., & Zhang, H. (2016). Palaeomagnetic results from Palaeogene red beds of the Chuan-Dian Fragment, southeastern margin of the Tibetan Plateau: Implications for the displacement on the Xianshuihe–Xiaojiang fault systems. *International Geology Review*, *58*(11), 1363–1381. https://doi.org/10.1080/00206814.2016.1157710

Wang, Y., Zhang, B., Schoenbohm, L. M., Zhang, J., Zhou, R., Hou, J., & Ai, S. (2016). Late Cenozoic tectonic evolution of the Ailao Shan-Red River fault (SE Tibet): Implications for kinematic change during plateau growth. *Tectonics*, *35*, 1969–1988. https://doi.org/10.1002/2016TC004229

Weil, A. B., Yonkee, A., & Sussman, A. (2010). Reconstructing the kinematic evolution of curved mountain belts: A paleomagnetic study of Triassic red beds from the Wyoming salient, Sevier thrust belt, U.S.A. *Geological Society of America Bulletin*, *122*(1-2), 3–23. https://doi.org/10.1130/B26483.1

Yang, Z. Y., Sun, Z. M., Ma, X. H., Yin, J. Y., & Otofuji, Y. (2001). Paleomagnetic study of the Early Tertiary on both Sides of the Red River Fault and its geological implications (in Chinese with English abstract). *Acta Geologica Sinica*, *75*, 35–44.

Yang, Z. Y., Yin, J. Y., Sun, Z. M., Otofuji, Y., & Sato, K. (2001). Discrepant Cretaceous paleomagnetic poles between Eastern China and Indochina: A consequence of the extrusion of Indochina. *Tectonophysics*, *334*(2), 101–113. https://doi.org/10.1016/S0040-1951(01)00061-0

Yao, H., Beghein, C., & Van Der Hilst, R. D. (2008). Surface wave array tomography in SE Tibet from ambient seismic noise and two-station analysis—II. Crustal and upper-mantle structure. *Geophysical Journal International*, *173*(1), 205–219. https://doi.org/10.1111/j.1365-246X.2007.03696.x

Yoshioka, S., Liu, Y. Y., Sato, K., Inokuchic, H., Su, L., Zamana, H., & Otofuji, Y. (2003). Paleomagnetism evidence for post–cretaceous internal deformation of the Chuan Dian Fragment in the Yangtze Block: A consequence of indentation of India into Asia. *Tectonophysics*, *376*(1-2), 61–74. https://doi.org/10.1016/j.tecto.2003.08.010

Zhang, B., Yin, C. Y., Zhang, J. J., Wang, J. M., Zhong, D. L., Wang, Y., et al. (2017). Midcrustal shearing and doming in a Cenozoic compressive setting along the Ailao Shan-Red River shear zone. *Geochemistry, Geophysics, Geosystems*, *18*, 400–433. https://doi.org/10.1002/2016GC006520

Zhang, B., Zhang, J., Chang, Z., Wang, X., Cai, F., & Lai, Q. (2012). The Biluoxueshan transpressive deformation zone monitored by syn-kinematic plutons, around the Eastern Himalayan Syntaxis. *Tectonophysics*, *574-575*, 158–180. https://doi.org/10.1016/j.tecto.2012.08.017

Zhang, B., Zhang, J., & Zhong, D. (2010). Structure, kinematics and ages of transpression during strain partitioning in the Chongshan shear zone, western Yunnan, China. *Journal of Structural Geology*, *32*(4), 445–463. https://doi.org/10.1016/j.jsg.2010.02.001

Zhang, B., Zhang, J., Zhong, D., Yang, L., Yue, Y., & Yan, S. (2012). Polystage deformation of the Gaoligong metamorphic zone: Structures, $^{40}Ar/^{39}Ar$ mica ages, and tectonic implications. *Journal of Structural Geology*, *37*, 1–18. https://doi.org/10.1016/j.jsg.2012.02.007

Zhang, Y. Q., Chen, W., & Yang, N. (2004). Ar-40/Ar-39 dating of shear deformation of the Xianshuihe fault zone in west Sichuan and its tectonic significance. *Science in China Series D-Earth Sciences*, *47*(9), 794–803.

Zhong, D.-L., Tapponnier, P., Wu, H.-W., Zhang, L.-S., Ji, S.-C., Zhong, J.-Y., et al. (1990). Large-scale strike-slip-fault—the major structure of intracontinental deformation after collision. *Chinese Science Bulletin*, *35*(4), 304–309.

Zhu, D.-C., Wang, Q., Cawood, P. A., Zhao, Z.-D., & Mo, X.-X. (2017). Raising the Gangdese Mountains in southern Tibet. *Journal of Geophysical Research: Solid Earth*, *122*, 214–223. https://doi.org/10.1002/2016JB013508

Zhu, R., Potts, R., Pan, Y. X., Lue, L. Q., Yao, H. T., Deng, C. L., & Qin, H. F. (2008). Paleomagnetism of the Yuanmou Basin near the southeastern margin of the Tibetan Plateau and its constraints on late Neogene sedimentation and tectonic rotation. *Earth and Planetary Science Letters*, *272*(1-2), 97–104. https://doi.org/10.1016/j.epsl.2008.04.016

Zijderveld, J. D. (1967). A. C. Demagnetization of rocks: Analysis of results. In D. W. Collinson, K. M. Creer, & S. K. Runcorn (Eds.), *Methods in paleomagnetism, Developments in Solid Earth Geophysics* (Vol. 3, pp. 254–286). New York: Elsevier. https://doi.org/10.1016/B978-1-4832-2894-5.50049-5